ERDC/CHL TR-24-14

Coastal and Hydraulics Laboratory

U.S. ARMY

US Army Corps of Engineers®

ERDC

Coastal Ocean Data Systems (CODS) and Coastal Inlets Research Program (CIRP)

Quantifying Coastal Evolution and Project Performance at Beaches by Using Satellite Imagery

Ian W. Conery, Nicholas R. Olsen, Shannon Brown, and Katherine L. Brodie

June 2024

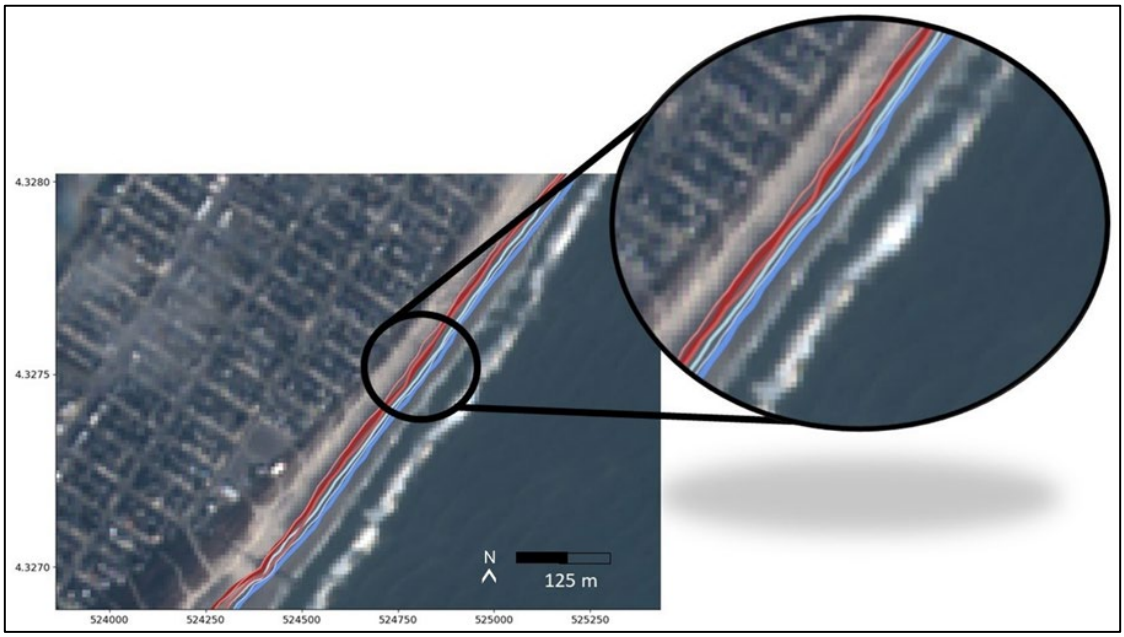

The US Army Engineer Research and Development Center (ERDC) solves the nation's toughest engineering and environmental challenges. ERDC develops innovative solutions in civil and military engineering, geospatial sciences, water resources, and environmental sciences for the Army, the Department of Defense, civilian agencies, and our nation's public good. Find out more at www.erdc.usace.army.mil.

To search for other technical reports published by ERDC, visit the ERDC online library at https://erdclibrary.on.worldcat.org/discovery.

ERDC/CHL TR-24-14
June 2024

Quantifying Coastal Evolution and Project Performance at Beaches by Using Satellite Imagery

Ian W. Conery, Nicholas R. Olsen, Shannon Brown, and Katherine L. Brodie

US Army Engineer Research and Development Center (ERDC)
Coastal and Hydraulics Laboratory (CHL)
3909 Halls Ferry Road
Vicksburg, MS 39180-6199

Final Report

Prepared for Coastal and Hydraulics Laboratory
3909 Halls Ferry Road
Vicksburg, MS 39180-6199

Under AMSCO 060000, “CODS/CIRP CoastSat”

Abstract

Accurately delineating the shoreline is crucial for tracking coastal evolution, community vulnerability, storm impacts, and for coastal management decision-making. However, existing shoreline measurement methods are often time-consuming and expensive and therefore, USACE Districts are often forced to narrow areas of interest or monitoring frequency, decreasing the likelihood of making data-driven management decisions, especially over regional scales. In the last decade, space-borne earth observations have captured images subweekly, and can potentially be used for shoreline monitoring. This work investigated the Python-based CoastSat toolkit and compared the shorelines derived from publicly available satellite imagery to ground truth surveys at 37 sites across the nation chosen in coordination with Districts. Mean horizontal errors ranged from 4.21 to 20.58 m with an overall mean of 11.32 m. Tidal corrections improved accuracies at 82% of sites. The CoastSat slope function was tested and there were negligible differences in shoreline accuracy when compared with user-defined slopes Twenty-year satellite-derived trends generally align well with ground truth trends. The satellite approach identified quantifying storm impacts and recovery, beach nourishment equilibration, diffusion and decay, shoreline response to nearshore berm placements and decadal shoreline evolution at the evaluated district sites. Work is ongoing to transition to a user-friendly software tool.

Contents

Figures and Tables

Figures

Tables

Preface

This study was conducted for the US Army Engineer Research and Development Center–Coastal and Hydraulics Laboratory (ERDC-CHL) Coastal and Ocean Data Systems; Coastal Inlets Research Program under AMSCO 060000, "CODS/CIRP CoastSat."

The work was performed by the Coastal Observations and Analysis Branch of the Flood and Storm Protection Division, ERDC-CHL. At the time of publication, Ms. Erin S. Diurba was branch chief; and Mr. David P. May was acting chief of the Flood and Storm Protection Division. The deputy director of ERDC-CHL was Mr. Keith Flowers, and the director was Dr. Ty V. Wamsley.

COL Christian Patterson was commander of ERDC, and Dr. David W. Pittman was the director.

1 Introduction

Coastal areas across the nation contain valuable historical, cultural, and natural resources that generate billions of dollars annually through tourism and industry (e.g., shipping and fishing). The position of the shoreline, generally defined as the land-sea interface, is a critical metric that is often used to track coastal evolution, community vulnerability, storm impacts and recovery, and for coastal management decision-making. Therefore, accurate delineation of the shoreline is crucial for coastal management decision-making (e.g., establishing construction setbacks). Yet, shorelines are complex and fluctuate on scales from seconds to decades, making measurements and predictions quite challenging.

1.1 Background

Within the US Army Corps of Engineers (USACE), frequent surveying of beaches and inlets is essential for understanding the relevant physical processes influencing sediment management and developing adaptive management strategies. Existing shoreline mapping techniques include GPS systems, airborne and terrestrial lidar, coastal video imaging, and unmanned aerial systems. However, these existing methods are often time-consuming and expensive and therefore, to conserve limited operational resources (e.g., personnel and vessels), USACE districts are often forced to narrow areas of interest or monitoring frequency, decreasing the likelihood of making data-driven management decisions. In the last decade, space-borne earth observations have captured images subweekly and can potentially be used to examine regional shoreline and inlet dynamics over subseasonal to multiyear time scales (e.g., Luijendijk et al. 2018; Xu 2018; Hagenaars et al. 2018; Bergsma et al. 2020). NASA launched Landsat 5 in 1984 offering advantageous long-term shoreline change context, and numerous global satellite missions with improved optical imaging sensors have since followed (Figure 1). Coastal data extraction from existing satellite observations would effectively incur no cost since the satellite imagery is publicly available, making it a low commitment choice for examining shoreline variability and preliminary planning for districts managing beach projects (e.g., Coastal Storm Risk Management) or inlets.

Figure 1. Major global civilian satellites and respective time lines.

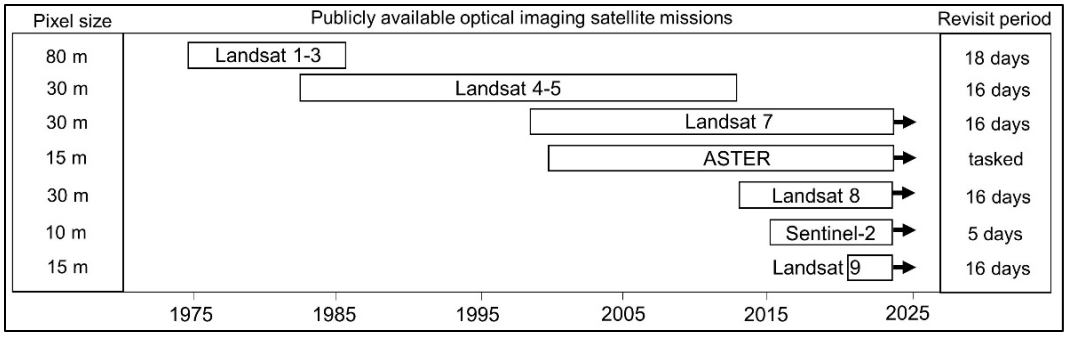

Using the normalized difference water index (NDWI) and machine learning algorithms, researchers have explored automated delineation of the boundary between land and sea in satellite imagery (Luijendijk et al. 2018; Hagenaars et al 2018). Success led to development of an open-source algorithm known as CoastSat which uses a supervised multilayer perceptron algorithm to classify the following four regions in a coastal image: *water*, *whitewater*, *sand*, and *other land features*. These classifications define the shoreline as the instantaneous interface between water and sand (Vos et al. 2019). CoastSat has been used to generate time series of coastlines around the world, providing insight into shoreline position (e.g., Vos et al. 2019) and beach slope (Vos et al. 2020). The CoastSat algorithm exists as a Python algorithm, which is not easily or efficiently accessible to most district users, thereby motivating the creation of a more user-friendly, transferable shoreline mapping tool. In addition, the algorithm has yet to be evaluated on many managed coastlines and so the ability to resolve rapid profile changes associated with nourishments needs to be rigorously investigated.

Development of this satellite-based tool offers the opportunity to both analyze and quantify natural coastal processes as well as the impacts of historic and future management strategies, such as nearshore berm placement and beach nourishments, on shoreline erosion rates at regional to national scales. Furthermore, these data could be used to help inform future survey extent and timing, or act as a supplement to typical crewed surveys or planned airborne lidar surveys, especially in remote or hazardous regions (e.g., USACE Jacksonville District [SAJ]–Puerto Rico). Shallow coastal inlets are notoriously dynamic (e.g., Velasquez-Montoya et al. 2020) and can be hazardous to navigate (e.g., recreational boating), due to varying sediment exchanges and shoaling processes which could be detectable from satellite data.

1.2 Objectives

The specific objectives of this overall effort are to (1) assess the ability of CoastSat to accurately quantify instantaneous shoreline positions and shoreline trends at a variety of USACE district sites by comparing to traditional ground-based survey methods and (2) to package the python-based satellite tool into a more user-friendly geographic information system (GIS) tool for districts (FY23). In this report we focus on documenting the results of objective one.

1.3 Approach

The remainder of this report will encompass (1) background on methodology (CoastSat and the Engineer Research and Development Center [ERDC] modifications), (2) test site and ground truth data descriptions, (3) instantaneous satellite shoreline accuracies compared to ground truth data, (4) long-term satellite shoreline trends, management applications, and storm impacts and recovery, and (5) conclusions and recommendations.

2 Methodology

This chapter outlines the process of using CoastSat with ERDC enhancements (Vos et al. 2019) to extract shorelines at various district test sites.

2.1 Image Preprocessing

CoastSat uses the Google Earth Engine (GEE) to download cropped imagery from Landsat 5, Landsat 7, Landsat 8, and Sentinel-2 missions, which began collections in 1984, 1999, 2013 and 2015, respectively (Figure 1) (Vos et al. 2019). The GEE streamlines image extraction, enables specific site selection and reduces the number of pulled spectral bands, significantly reducing download file sizes. The Landsat missions and Sentinel-2 have revisit times of 16 and 5 days, respectively. Despite differences in satellite resolution (Figure 1), where Landsat missions range from 30 m to 80 m and Sentinel-2 collects at 10 m, a multistep technique was employed in CoastSat to create consistent spatial resolution across all satellite images.* With the imagery downloaded, a multiband raster data set is created by fusing the high resolution sharpened panchromatic band that spans multiple spectral bands (Landsat 7 and Landsat 8) and the lower resolution from other sensors, effectively improving the spatial resolution from 30 to 15 m (Vos et al. 2019). Because of the absence of the panchromatic band in Landsat 5 and Sentinel-2, a subpixel down sampling technique was applied to make comparable image resolution and spatial error among all four satellite images (Vos et al. 2019). When cloud cover exceeds 10% in images they are automatically excluded.

2.2 Transect and Baseline Construction

The user is prompted to draw a reference shoreline from the first image of sufficient quality from the series. This reference line is the basis of comparison for the machine learning (ML) detected shorelines and used to identify good shorelines from the ML set. A detected shoreline point exceeding a distance of 150 m from the reference line is eliminated from the collection of detected points made for each image.

* For a full list of the spelled-out forms of the units of measure used in this document and their conversions, please refer to *US Government Publishing Office Style Manual*, 31st ed. (Washington, DC: US Government Publishing Office, 2016), 248–52 and 345–47, https://www.govinfo.gov/content/pkg/GPO-STYLEMANUAL-2016/pdf/GPO-STYLEMANUAL-2016.pdf.

Reference baselines are constructed across each of the study sites landward of the landward-most satellite-derived shoreline. Cross-shore transects are cast perpendicular from the reference line every 1.0 m in the alongshore as chosen by the research team. To calculate shoreline change, the intersection of each transect with each shoreline is extracted and differenced. The transect-based approach allows for the calculation of shoreline change in both the cross-shore and alongshore dimensions. A second transect collection is also produced as specified by the research team, subset from the first, with a transect every 70 m. This reduced collection of transects offers adequate spatial resolution with significant performance improvements and therefore, is used in most subsequent ERDC statistical analyses. However, users can use the 1.0 m-spaced transects if needed.

2.3 Shoreline Extraction

CoastSat employs a multistep shoreline extraction process. A manually digitized training data set from five sites using 1,500 pixels per class and accuracy of 98% was used to formulate supervised classification to categorize each pixel as *sand*, *water*, *whitewater*, or *other* (Vos et al. 2019). Next, the modified NDWI (MNDWI) creates a grayscale image and calculates values between –1.0 and 1.0 for each pixel, where positive values represent land and negative represent water. Otsu's thresholding algorithm is used to optimize the distinction between land and water and the iso-valued contour shoreline is drawn using the marching squares technique (Vos et al. 2019). The shoreline extraction methodology was trained and tested at the following five sites with varying wave and tidal conditions and beach slopes: Narrabeen, Australia; Moruya, Australia; Tairua, New Zealand; Duck, North Carolina; and Truc Vert, France with root-mean-square errors (RMSE) of 8.2 m, 11.6 m, 7.3 m, 9.0 m and 12.7 m, respectively.

The open-source CoastSat analysis requires the user to manually select images of adequate quality prior to the shoreline delineation step above (e.g., cloud presence). This process, performed for every image, could take an hour or more to evaluate a site over a typical one to two decade analysis. To reduce user workload, ERDC developed a simple machine-learning based tool to high- and poor-quality bypass this step and filter out poor images and resultant shorelines. This tool was trained from sorted image and shoreline combinations that were performed by hand

previously in the project. The training set included over 1,000 usable shorelines and over 500 unusable shorelines.

The ERDC-modified version of CoastSat relies on the coordinates that define the shape of the CoastSat-determined shoreline associated with each image. To train a *k*-nearest neighbors voting algorithm the shoreline length and Hausdorff distance is calculated from the already classified sites. This results in a binary classifier using the deviation of those attributes in an unclassified shoreline from a small set of user-selected high quality shorelines.

For the user this means that after a series of initial judgements provide the algorithm with sufficient information, it is capable of sorting most of the remaining shorelines independently. We have also included a check on the algorithm where after fifty independent classifications, the user is prompted to make a few more decisions to ensure that the shoreline standard is maintained despite evolution of the coastline over the analysis period. The user can conduct quality assurance and quality control (QAQC) and rerun the algorithm iteratively.

The shorelines produced by the CoastSat ML algorithm are a connected series of points, each of which represents a pixel that was determined to represent the interface of land and water (Vos et al. 2019). Of interest is the shoreline, but other valid interfaces may be detected as well, including swimming pools, lagoons, landscaping features, etc. Invalid interfaces may also be found including white or reflective rooftops, particularly dense clouds, etc. When the series of points is drawn together to form a linear shoreline feature these extraneous detections can cause double shorelines, offshoots, loops, and other problematic geometries. Not all of these are detected in the bad shoreline sorting above, nor is that desired, as many accurate shoreline delineations could be lost due to the presence of a static structure like a swimming pool. To reduce the quantity of data that must be discarded, a cleaning function was developed by ERDC. This function takes each set of shoreline points and measures the distance from point-to-point along the series. Clusters of points occurring more than 100 m away from the longest string of neighboring points are discarded. These cleaned shorelines are saved as a shapefile at this step.

2.4 Beach Slope and Tidal Correction

CoastSat extracts the position of the wet and dry boundary, and therefore is influenced by the prevailing water level. Since the time of the image is known, a tidal correction is possible using Equation (1),

$$\Delta x = \frac{z_{ref} - z_{wl}}{m}, \quad (1)$$

where

Δx = cross-shore horizontal shift along the shore-normal transects,
z_{ref} = reference elevation (e.g., 0.0 m above mean sea level),
z_{wl} = local water level (tide + residuals) at the time of image acquisition (stored in metadata), and
m = beach face slope. Positive Δx infers offshore direction.

Note, the tidal correction is site-specific and therefore not implemented in the standard CoastSat toolbox but added as an ERDC enhancement.

To initiate the tidal correction, ERDC added automatic selection of the closest NOAA tidal station. Since the closest station is not always satisfactory, the user can also input a choice of station. For each satellite pass a daily 6-minute series is downloaded from the NOAA server.

Following this, if the user has not provided an estimate of the beach slope, the CoastSat.Slope module is used to determine the beach slope by calculating the energy inside the peak tidal frequency band for a power spectrum density of a range of hypothetical tidally corrected time-series of shorelines (Vos et al. 2019). The minima of the integrated spectra are expected to most closely match the actual beach slope (Vos et al. 2019). The average beach slope, whether given by the user or CoastSat.Slope is then used to shift both the shoreline shapefile and the cross-shore distances table. This operation converts the previous land and water interfaces which only have a horizontal spatial orientation to a proper shoreline with an associated vertical datum as well; in this case NOAA's mean sea level. Users should be aware that the CoastSat.Slope used to shift shorelines applies only the intertidal region.

2.5 Wave Runup Correction

A correction for wave runup was explored as an addition by the team. The wave height closest to the time of each satellite pass is taken from a user-selected NOAA National Data Buoy Center (NDBC) buoy. Stockdon's 2006 standard runup, Equation 2, is used to calculate the wave's vertical displacement from the significant wave height delivered by the buoy,

$$R_2 = 1.1\left(0.35\beta_f(H_0L_0)^{1/2} + \frac{[H_0L_0(0.563\beta_f^2+0.004)]^{1/2}}{2}\right), \quad (2)$$

where

H_o = wave height,
L_o = wavelength, and
β_f = beach slope.

These vertical dimensions from waves are used in the same manner as the tidal elevation correction above, to shift the shoreline along a given slope. The runup correction is a positive value, indicating height above the still water level, leading the runup correction to only move shorelines seaward, that is, to negate the falsely derived, more landward shoreline resulting from wave runup.

3 Site Selection

The research team aimed to select sites that encompassed a broad range of coastal settings and environmental conditions (Figure 2 and Table 1). First, USACE districts were contacted for recommendations based on (1) areas with robust shoreline survey ground truth data, (2) areas with management challenges or beach projects (e.g., nourishments and nearshore berms), and (3) areas where traditional surveys may be difficult or costly making supplementary satellite data useful.

Figure 2. Test sites (*stars*) chosen in coordination with US Army Corps of Engineers (USACE) districts. (Image reproduced from Google ©2023.)

Table 1. Summary characteristics from test sites.

Test Site	Sig. Wave Height (m)	Avg. Wave Period (s)	Tidal Range (m)	Ground Truth	Mgmt. Action
Lake Michigan	n/a (not applicable)—wind swell	n/a	n/a	29 unmanned aerial vehicle (UAV) topo. surveys	n/a
Avalon, New Jersey	0.8	8.3	1.3	11 cross shore profile shorelines	Nourishments, truck hauls
Stone Harbor, New Jersey	0.8	8.3	1.3	11 cross shore profile shorelines	Nourishments, truck hauls
Duck, North Carolina	1.0	7.5	1.0	407 cross shore profile shorelines	Unmanaged

Table 1 (cont.). Summary characteristics from test sites.

Test Site	Sig. Wave Height (m)	Avg. Wave Period (s)	Tidal Range (m)	Ground Truth	Mgmt. Action
New Smyrna Beach, Florida	1.5	8.3	1.4	12 Mini Argus shorelines	Nearshore berm placement
Galveston, Texas	0.5	5.3	0.9	5 Lidar shorelines	Nourishments, berm placements
Padre Island, Texas	1.1	6.0	0.9	5 Lidar shorelines	Nourishments, groins, geotextile tubes
Imperial Beach, California	0.9	13.0	2.2	124 DEM[1] shorelines	One small nourishment
Cardiff, California	1.0	13.6	2.2	124 DEM shorelines	One small nourishment, rip rap
Torrey Pines, California	1.0	13.2	2.2	124 DEM shorelines	One small nourishment
Benson Beach, Washington	2.2	11.0	3.1	84 DEM shorelines	n/a
Harvey Cedars, New Jersey	0.9	6.4	1.3	9 cross shore profile shorelines	Nourishments, Nearshore berm

1. DEM = digital elevation model.

3.1 Lake Michigan, Illinois

In the interest of testing a lacustrine shoreline, the research team coordinated with the Chicago District and Michigan State University (Dr. Ethan Theuerkauf; Department of Geography, Environment, and Spatial Sciences) to obtain ground-truthed shoreline data along Lake Michigan. The testing site is located along the southwestern shoreline of Lake Michigan in northeastern Illinois and is part of the Illinois Beach State Park. The shoreline is composed of sand as a ridge and swale complex (Theuerkauf et al. 2019). An outwash deposit was reworked around 4,500 years before present into a strandplain beach and has been characterized by erosion in the northern portion (this site) and accretion to the south through predominant southerly alongshore transport of eroded sediment. Sensitive to fluctuating lake levels (Figure 3), the beach ridges have experienced cyclic destruction and formation where low lake levels promote growth and high levels trigger erosion (Fraser et al. 1990). In the late 1800s, jetties and other stabilization structures were constructed to the south to slow the net southerly migration of the beach ridge complex (Chrzastowski et al. 1996). After low water levels in the early 2000s, the lake rose rapidly at over 0.5 m over six months in 2014 (Figure 3, *red circle*), resulting in accelerated

erosion and habitat loss. The specific testing site is characterized by a narrow, approximately 10 m beach, and a small foredune (<1.5 m) which makes it susceptible to overwash (Figure 4).

Over the 6 km testing site, 29 unmanned aerial vehicle (UAV) surveys were collected by the Theuerkauf group between July 2018 and January 2021, with the goal to evaluate the hydrodynamic conditions responsible for rapid erosion, specifically whether water levels alone are the primary control or whether certain wave conditions are also a significant factor. A DJI Phantom 4 Pro quadcopter was used to collect high resolution imagery (20 megapixel) with 80% overlap and Agisoft Metashape was used for structure-from-motion photogrammetry. Ten to fifteen ground control points were evenly spaced throughout the site and were surveyed using a Trimble GEO 7X GPS system and RSMEs of the constructed elevation surface were less than 5 cm. Shorelines were digitized from these robust elevation surfaces based on the land and water interface from the edges of the point clouds and ortho imagery.

Figure 3. Lake Michigan water level fluctuations since 1918. *Solid red line* represents long-term average. (Image reproduced from USACE 2023. Public domain.)

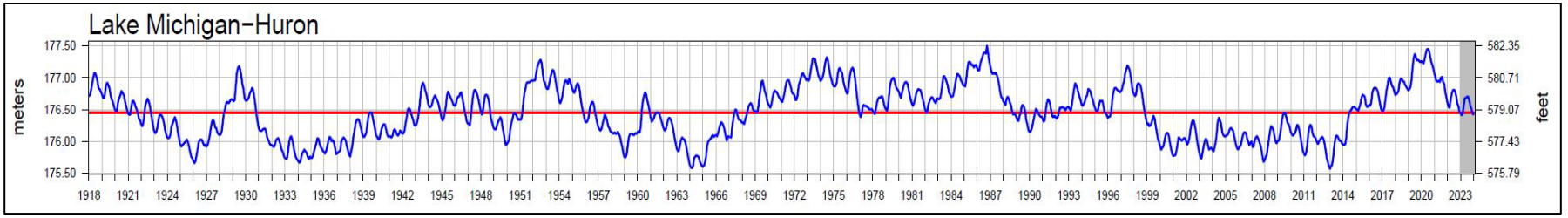

Figure 4. Unmanned aerial vehicle (UAV) imagery collected from the beginning and end of the study used for ground truth shoreline data. Note the strong erosion over the time interval and loss of the road (*gold arrow*).

3.2 Avalon and Stone Harbor, New Jersey

Avalon and Stone Harbor, New Jersey, are located on a barrier island on the Atlantic Ocean coast of New Jersey, bound by Townsends Inlet to the north and Hereford Inlet to the south (Figure 5). During the Quaternary Period, sea level changes caused the spreading of sand and gravel deposits that have been reworked through time. The Cape May formation in particular was deposited along valley bottoms and estuarine and marine zones to form the shoreline during the last interglacial when sea level was approximately 10 m higher than present. The average wave height in the region is 0.8 m with a wave period of 8.3 s (Thompson 1977). The tides are semidiurnal with a range of 1.3 m (Dally and Osiecki 2018).

Subject to major flooding and erosion during storms, a feasibility study for mitigation over a 15-mile stretch began in 1992. The first coastal storm risk management (CSRM) project was constructed in 2002 by USACE at each town. While a three-year renourishment interval was authorized, there was not sufficient federal funding for renourishment until 2016. As a federal alternative, the Borough of Avalon, sometimes in partnership with the New Jersey Department of Environmental Protection, placed 2.4 M yd^3 of sand between 2005 and 2016 along the erosional hotspot of Avalon (Figure 5). In addition, USACE added truck hauls (2009) and emergency beachfills (2011 and 2013) totaling 961,000 yd^3. The last nourishment of 1,636,685 yd^3 was conducted in 2017.

Beginning in 2002, 56 profile lines were surveyed from the dune through the depth of closure using a combination of GPS, ATV and boat data for a nourishment feasibility study. The ground truth for satellite shoreline comparison consists of 11 shorelines collected between 2002 and 2019 which were generated using the original 56 beach profiles from 2002 with the addition of three profile lines.

Figure 5. Oblique aerial photograph looking southwest of the Avalon, New Jersey, study site.

3.3 Duck, North Carolina

Duck, North Carolina, is located on a narrow and long barrier island on the Atlantic coastline in the northern Outer Banks in North Carolina (Figure 6). Tides are semidiurnal with a mean range of approximately 1 m and mean significant wave height is 1.0 m ± 0.6 m (Lee et al. 1998). Duck is prone to high wave energy in the winter from nor'easters, or extratropical systems, and hurricanes in the summer and fall months. Dominant longshore transport is from north to south and is largely storm driven (Dolan et al. 1988). An artificial dune was constructed in the 1930s and 1940s to protect the roadway (Birkemeier et al. 1984).

Figure 6. Duck, North Carolina, 2017 beach nourishment. USACE Field Research Facility research pier is visible at the top of the frame. (Image reproduced with permission from the Town of Duck and Coastal Planning and Engineering of North Carolina.)

The USACE Field Research Facility (FRF) was constructed in Duck in the late 1970s and has since been a world-renowned coastal observation facility (Figure 6). The FRF has the unique ability to collect data within the challenging surf zone using amphibious vessels and custom instrumentation. The monthly subaqueous and subaerial survey of the property (1 km long) has been a staple of the FRF observational record since the early 1980s (Birkemeieir et al. 1984). Profile data from these frequent monthly surveys is highly accurate (approximately 3 cm error; Forte et al. 2017) and was used for comparison with satellite-derived shorelines. Duck was nourished for the first time in 2017 (1.0 M yd^3) and the project stopped at the northern property boundary of the FRF, allowing for an opportunity to monitor project equilibration and longshore diffusion of the added sand.

3.4 New Smyrna Beach, Florida

New Smyrna Beach is located on a barrier island on the Atlantic Coast in central Florida (Figure 7). Ponce de Leon Inlet is located just north of the town and experiences problematic, chronic shoaling, requiring regular dredging. This region of central Florida is characterized predominantly of

Holocene barrier deposits and dominant longshore transport is southerly with a seasonal reversal to the north in the summer (Stapor and May 1983).

Figure 7. New Smyrna Beach and location of dredge and nourishment activities. (Image adapted from Bruder et al. 2019. Creative commons CC BY 4.0.)

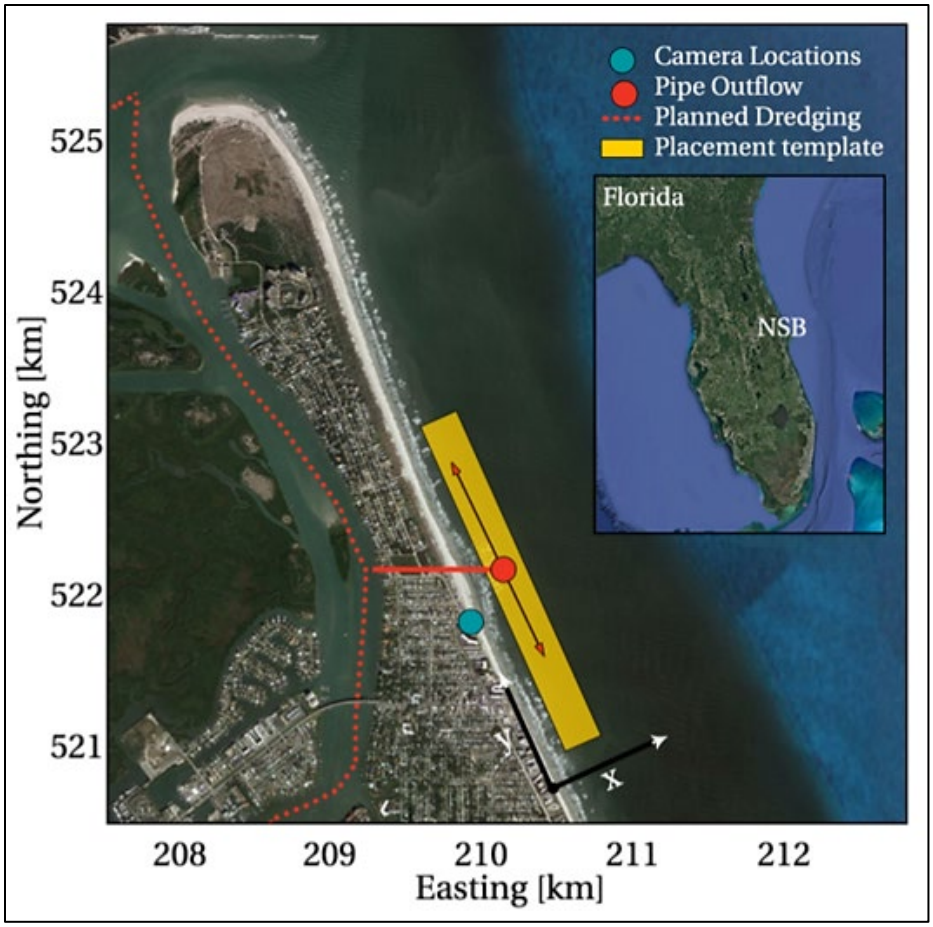

New Smyrna Beach has historically been affected by hurricanes and nor'easters, causing extensive shoreline erosion. From August 2018 through March 2019, 350,000 m^3 of sediment was dredged from Ponce De Leon Inlet to reduce shoaling and was placed via pipeline in the nearshore of New Smyrna Beach at approximately 4 m water depth (Figure 7) (Onnink 2020). This nearshore berm nourishment was monitored hourly by ERDC Coastal Hydraulic Laboratory (CHL) researchers using a mini-argus camera system mounted on a high-rise building consisting of four cameras collecting snapshot, timelapse, variance, and brightest and darkest imagery from August 2018 to September 2019 (Figure 8) (Bruder et al. 2019). Specifically, shorelines were manually digitized using the georectified timex imagery following methods outlined in Bruder et al. (2019). The manual digitization approach is estimated to have a precision on the order of 10 m (Onnink

2020). Timex imagery is time-averaged during the collection time (10 min) and has been successfully used in the past for extracting shoreline positions (Lippmann and Holman 1989; Holman et al. 1993). During the deployment, significant wave height was 1.5 m, mean wave period was 8.3 s, and the maximum tidal range was 1.4 m.

Figure 8. Timex imagery from the Coastal Ocean Data Systems (CODS) mini-argus deployment from (*top* to *bottom*) 1 September 2018, 15 September 2018, 1 November 2018, and 2 February 2019 capturing various stages of evolution following the nearshore berm placement. "SPAW" represents shoreward propagating accretionary wave. (Image reproduced with permission from Onnink 2020.)

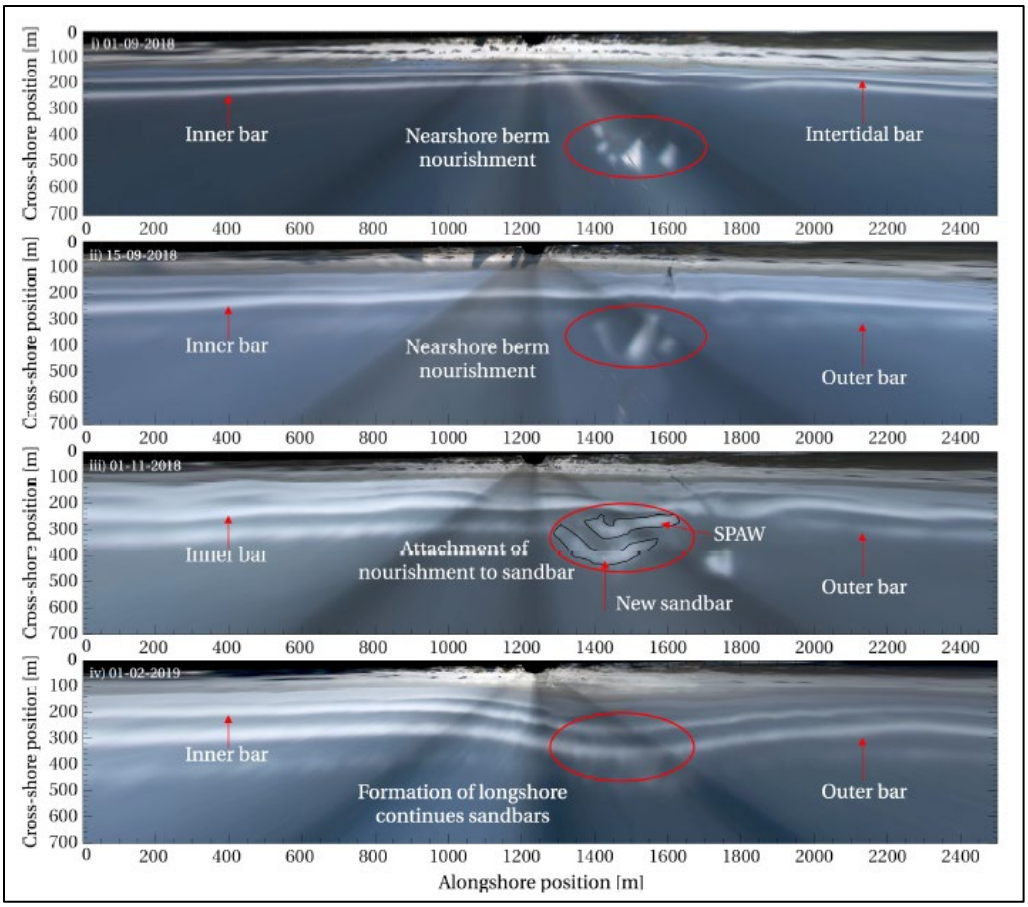

3.5 Galveston and Padre Island, Texas

An extensive study by the Texas Bureau of Economic Geology (Paine et al. 2021) found significant net coastal retreat on Galveston and Padre Islands, Texas, both tourist destinations that represent valuable habitat, industrial infrastructure and economic resources to the state. Because of the shoreline behavior and management challenges, the Galveston District recommended the sites for satellite testing.

The Texas Coast is characterized by complex geologic history. The shoreline position is a function of multiple related coastal processes including sea level change, land subsidence, sediment influx, littoral drift, and storm impacts and recovery (Paine et al. 2021). The coastline includes the Holocene geomorphic features of barrier islands, strandplains, fluvial and deltaic headlands, and chenier plains (Aronow et al. 1982; Brown et al. 1975; LeBlanc and Hodgson 1959). Three major rivers affect hydrodynamics and sediment supply along the coast (Brazos, Colorado, and Rio Grande), although construction of dams for flood control and water supply have reduced sediment loads. During the Holocene transgression, Galveston Bay formed landward of the barrier islands as Pleistocene river valleys were submerged. A convergence zone occurs at Padre Island where currents generated from southeasterly winds meet the Rio Grande deltaic headland to the south and the Brazos-Colorado headland to the northeast. Relative sea level rise is a major factor influencing coastal processes along the Texas Coast, and the Galveston Pier 21 has the longest period of water level record showing a long-term rate of sea level rise of 6.55 mm/yr (between 1904 and 2019). The Texas coast was affected by a plethora of tropical storms through time, notably Hurricane Ike (2008) and Hurricane Harvey (2017).

According to district records, a total of 20 beach projects were conducted between 2000 and 2021 for Galveston and Padre Island beaches. Of these projects, five included placement of less than 6,000 yd^3. Three projects were related to dune construction and the placement of geotextile tubes (2000, 2007, and 2009). The largest project was conducted in 2017 involving 1 M yd^3 of nourishment throughout the Galveston groin field. At South Padre Island, a total of 15 beach projects were completed between 2000 and 2021. Of those, seven were berm placements and eight were nourishments. Placement volume ranged from 220,000 yd^3 to 500,000 yd^3. The eastern portion of the Galveston shoreline includes a series of groins for sediment capture, which has created distinct shoreline configuration (Figure 9).

Shoreline positions were extracted from airborne lidar topographic data sets from 2010, 2011, 2012, 2016, and 2019 (Paine and Caudle 2020). Shorelines were delineated at an elevation contour from the 1 m resolution digital elevation model (DEM) that approximate the wet beach / dry beach boundary consistent with historical use in shoreline studies. This wet / dry interface was checked by superimposing the lidar data on georectified

National Agricultural Imagery Program aerial imagery (Paine and Caudle 2020). Lidar data were georeferenced and compared to GPS-derived ground control points and calibration targets. All lidar surveys were flown in late winter or spring, other than the 2016 survey that was conducted in fall.

Figure 9. Oblique aerial image of Galveston Island. Note the numerous jetties. (Image reproduced from Flickr. Creative Commons BY-NC-SA 2.0.)

3.6 San Diego Beaches, California

In coordination with USACE, Scripps Institute of Oceanography has collected long-term, high resolution subaerial and subaqueous coastal monitoring data sets. In 2019 Ludka et al. (2019) published a summary paper and released a data set covering three reaches of San Diego coastline (Torrey Pines, Cardiff, and Solana). The data span between eight to 16 years (2001–2016) and spatial extents vary from 4.2 km to 7.9 km in the alongshore. For this work, monthly to quarterly topographic surveys at 100 m spaced cross-shore transects were used to extract the shoreline position for comparison to satellite data.

This region of coastline is hydrodynamically and geologically complex (Ludka et al. 2019). Rocky headlands, nearshore submarine canyons and offshore shoals contribute to alongshore wave variability, in addition to the nearby Channel Islands that create shadowing and refraction effects

over variable shelf bathymetry. Generally, the winter season produces the most energetic waves from the North Pacific and promotes southerly longshore sediment transport and the milder summer South Pacific swell causes shoreward and northerly transport. Sea cliffs back much of the coastline and are composed of a bottom unit of lithified Eocene and Miocene mudstone, shale, sandstone, and siltstone, and a top unit consisting of unlithifed Pleistocene terrace deposits. Cobbles are intermittently exposed along the beaches, most often when beach sands are eroded (Ludka et al. 2019).

The Torrey Pines stretch contains reef, a lagoon mouth, and the landward tip of the Scripps Submarine Canyon. In 2001 monitoring was initiated to capture the evolution of a subaerial beach nourishment project constructed in 2002 to protect an adjacent major roadway. Data showed rapid (monthly) transport of the nourished sediment to an offshore bar followed by the partial return of the sediment through onshore transport in the summer. Much of this region is characterized by cobble (Figure 10).

The majority of Cardiff and Solana also contain reef and have lagoon mouths at the northern and southern boundaries. While Solana is backed by cliffs, Cardiff contains rip rap to stabilize the roadway and parking lots that are often flooded (Figure 10). In 2012, both beaches were nourished and observations showed minimal loss of the sediment from the subaerial beach over the course of a few years.

Imperial Beach contains the Tijuana River Mouth and offshore cobble shoal to the south, along with a recreational pier and two short jetties (100 m to 150 m) to the north. Some homes are protected by riprap and small dunes (Figure 10). This beach was also nourished in 2012 and had similar success to Cardiff and Solana, yet eventually the nourished material was transported to the river mouth causing problematic clogging and consequent degradation of water quality in the estuary (Ludka et al. 2019).

Figure 10. Low tide photos of Cardiff, Torrey, and Imperial Beaches. (Image reproduced from Ludka et al. 2019. Creative Commons CC BY 4.0.)

The subaerial survey data were collected with an ATV (shocks removed and constant tire pressure) at low tide in combination with a push dolly, both outfitted with high precision Global Navigation Satellite System (GNSS). Subaqueous data were acquired with a personal watercraft outfitted with a 192 kHz acoustic sonar, a sea surface thermistor for speed of sound calculations, and GNSS antenna. The combination of the three methods ensured continuous profile overlap across the surf zone (Ludka et al. 2019).

3.7 Benson Beach, Washington

The high wave energy coupled with large sediment-laden river systems in Washington State creates many dynamic coastlines. With input from several district engineers, Benson Beach at the mouth of the Columbia River (Figure 11) was selected for satellite validation, primarily due to dense data availability over the past two decades and history of challenges in managing the stretch of coast. Beginning in 1996, the Washington Department of Ecology in conjunction with the US Geological Survey, and Oregon State University, spearheaded a comprehensive coastal monitoring program for the state, generating frequent high resolution morphology data sets. According to Ruggiero et al. (2003; p. 59) The primary goals of the study were to "improve scientific understanding of coastal morphodynamics and sedimentary processes, to determine natural and anthropogenic influences of the littoral system, and to provide information and predictions of coastal behavior at temporal scales of decades and spatial scales of tens of kilometers." In addition, these data enable the testing and development of hydrodynamic and sediment transport models in the region.

The Columbia River Littoral Cell (CRLC) extends between Tillamook Head, Oregon, and Point Greenville, Washington. Two large estuaries, Willapa Bay and Grays Harbor, lie to the north. A relatively slow rate of eustatic sea level rise approximately 6,000 years ago caused the formation

of modern barrier islands and strandplains as the shelf and estuary filled (Kaminsky et al. 2010). Beaches began to prograde about 4,500 years ago. Situated along an active tectonic margin, earthquakes have caused coastal subsidence and shoreline retreat over an estimated 500-year recurrence interval (Kaminsky et al. 2010). Yet despite the seismic influence, the coastlines have been net progradational due primarily to high sediment load delivered from the Columbia River that is redistributed by the strong wave climate. The Pacific Northwest is notorious for a severe wave climate, generally producing significant wave height—approximately 10 m high and long period (13 s)—winter storm waves at least once annually. The combination of high wave climate and fine-grained sands gives the CRLC a morphodynamic classification of modally dissipative (Wright and Short 1984; Ruggiero et al. 2005), dominated by low-frequency infragravity energy in the nearshore zone. Tides are mixed semidiurnal ranging from 2 m to 4 m (mesotidal). Driven by winter wave and wind energy, the net sediment transport is to the north (Kaminsky et al. 2010).

Figure 11. Benson Beach, Washington. Notice the narrow, steep beach and storm-deposited debris. (Image reproduced from M. Hanscom 2007. Flickr. Creative Commons BY-NC-SA 2.0.)

The comprehensive monitoring program contains the primary components of cross-shore topographic beach profiles, 3D topographic beach surface maps and nearshore bathymetry. For this study, researchers obtained 84 beach surface maps collected roughly biannually to quarterly from 1997 to 2019. The site was nourished in 2002 (43,000 yd^3). Data

were collected with an ATV equipped with survey grade D-GPS receiver, GPS antenna, radio modem, radio antenna, data logger, and cabling to the real-time kinematic (RTK) backpack that is also used for typical beach profile surveys. Differential corrections were provided by a geodetically fixed RTK GPS base station. Data points were densely spaced in the alongshore to resolve small scale features (e.g., cusps and berms) and cross-shore transect spacing was on the order of approximately 10 m, although drivers used discretion to determine the most optimal path for capturing the variability of features. The ATV data collection spanned from the foredune toe to the swash zone. Data were manually checked for quality, then Matlab scripts were used by Washington Department of Ecology to map nonuniformly spaced raw data onto a 2D gridded surface through weighted linear interpolation. Comparisons with robust beach profile surveys show that the vertical RMS error of the ATV interpolated beach surface is typically less than 5 cm in the horizontal dimension and 10 cm in the vertical dimension.

3.8 Harvey Cedars, New Jersey

Harvey Cedars is located on a barrier island on the Atlantic Coast in central New Jersey. The beach is roughly 3 km long and faces east / southeast. Average wave heights in the region are 0.9 m and average wave period is 6.4 s (Cialone and Thompson 2000). The tides are semidiurnal with a range of 1.3 m (Dally and Osiecki 2018).

Identified as an erosional hotspot, CSRM has constructed groins and the first project in 2010. Since this project, three renourishments have followed including emergency repair from the impacts of Hurricane Sandy. The last, most recent management project at Harvey Cedars was the emplacement of a nearshore berm. In the summer of 2021, 83,300 m^3 was dredged from Barnegat Inlet and placed in the nearshore (–2.75 m North American Vertical Datum of 1988 [NAVD 88] depth) of Harvey Cedars by the USACE Philadelphia District (NAP). Water Resources Development Act (WRDA) Section 1122, program supports experimental beneficial use projects such as this effort. Nine topographic and bathymetric surveys conducted during this project serves as ground truth for satellite comparisons. RTK-GPS and single beam transects were spaced every 75 m (26 total) and combined to create DEMs. Work to analyze the evolution of the placement is ongoing using in situ hydrodynamic sensors and satellite-derived shorelines (McGill et al. 2022).

4 Instantaneous Shoreline Comparisons

A primary goal of this effort was to quantify the accuracy of CoastSat using ground truth data from test sites across the nation. Overall, across all sites the mean horizontal difference from the ground truth shorelines was 14.1 m (Figure 12). However, Figure 12 highlights the variability in the skill where mean horizontal differences from ground truth ranged from 4.8 m to 32.0 m. Interestingly, individual sites within the same study area also performed at varying accuracy. For example, mean horizontal differences at adjacent sites on South Padre Island ranged from 4.79 m to 21.31 m (Figure 12). The Lake Michigan region also exhibited variability in accuracy performance with a range of 9.09 m to 17.84 m in mean horizonal difference. This regional variability in accuracy may be due to several potential factors including image coregistration differences across the region.

The results of this work use output from CoastSat V1. During this effort, our research team and the CoastSat creator (K. Vos, pers. comm. 24 August 2024) each discovered coregistration issues related to Google Earth Imagery ingestion that was essentially rounding area of interest polygons and resulted in offsets among satellite missions (Figure 13). This issue has since been partially corrected in CoastSat V2.

Sites where this problem is evident have been starred in Figure 12. Since this report focuses on the performance of the CoastSat algorithm, and the issue is associated with GEE, we have omitted results from the problematic sites from subsequent analysis. When these sites are not included, the overall mean horizontal difference between satellite-derived shorelines and ground-truth shorelines is reduced to 11.32 m.

Figure 12. Summary of mean horizontal difference (offset) of satellite-derived shorelines compared to ground truth surveys across test sites. *Yellow stars* indicate sites with an apparent Google Earth Engine (GEE) imagery issue that will be omitted from subsequent analysis.

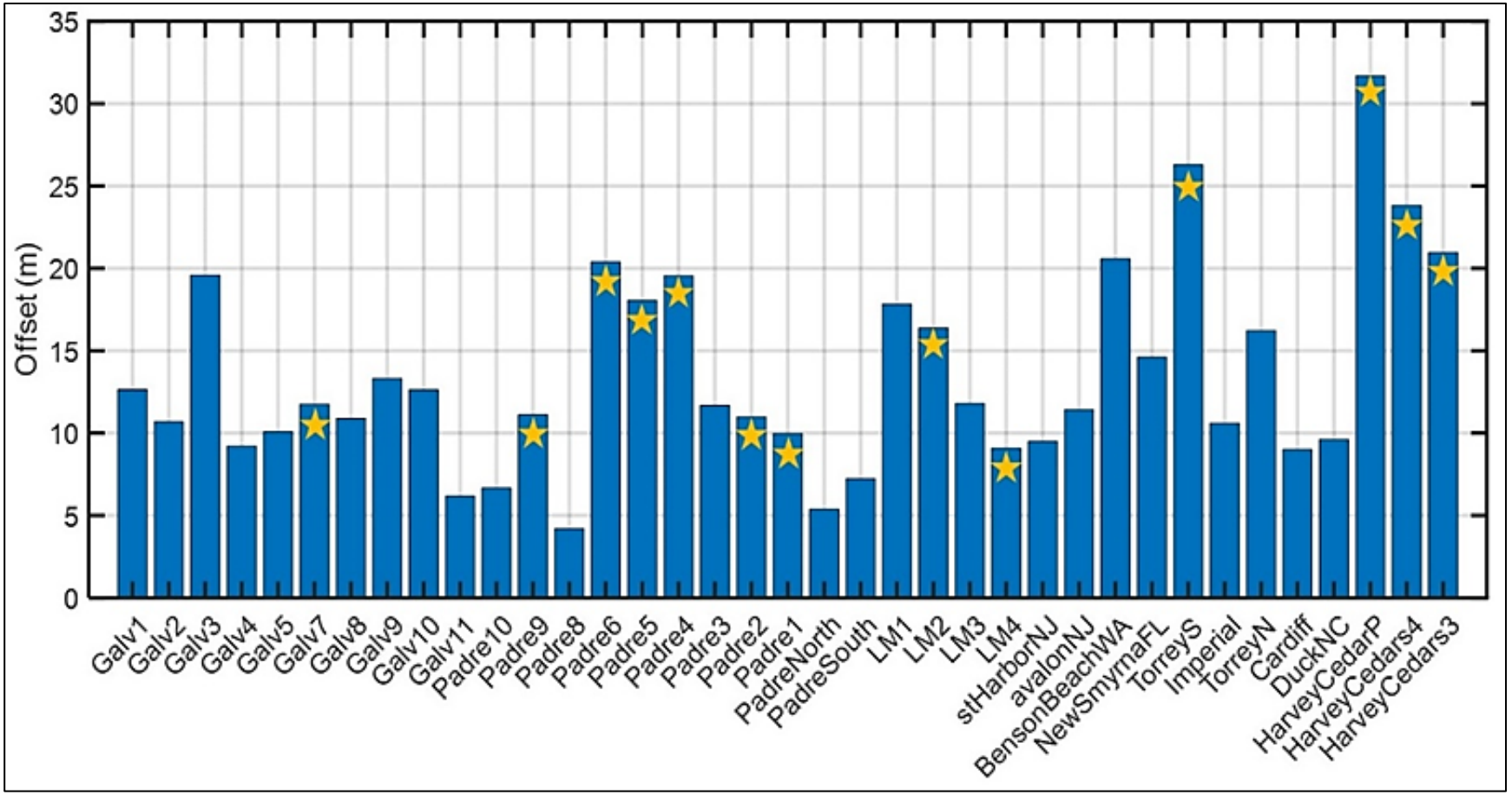

Figure 13. Shoreline positions through time for Padre3 (*a*), Padre4 (*b*), and Harvey Cedars Pilot (*c*). Points are colored based on satellite mission. Notice good alignment across missions in panel *a* and misalignment of Landsat 8 (*red*) and Sentinel-2 (*blue*) in panels *b* and *c*.

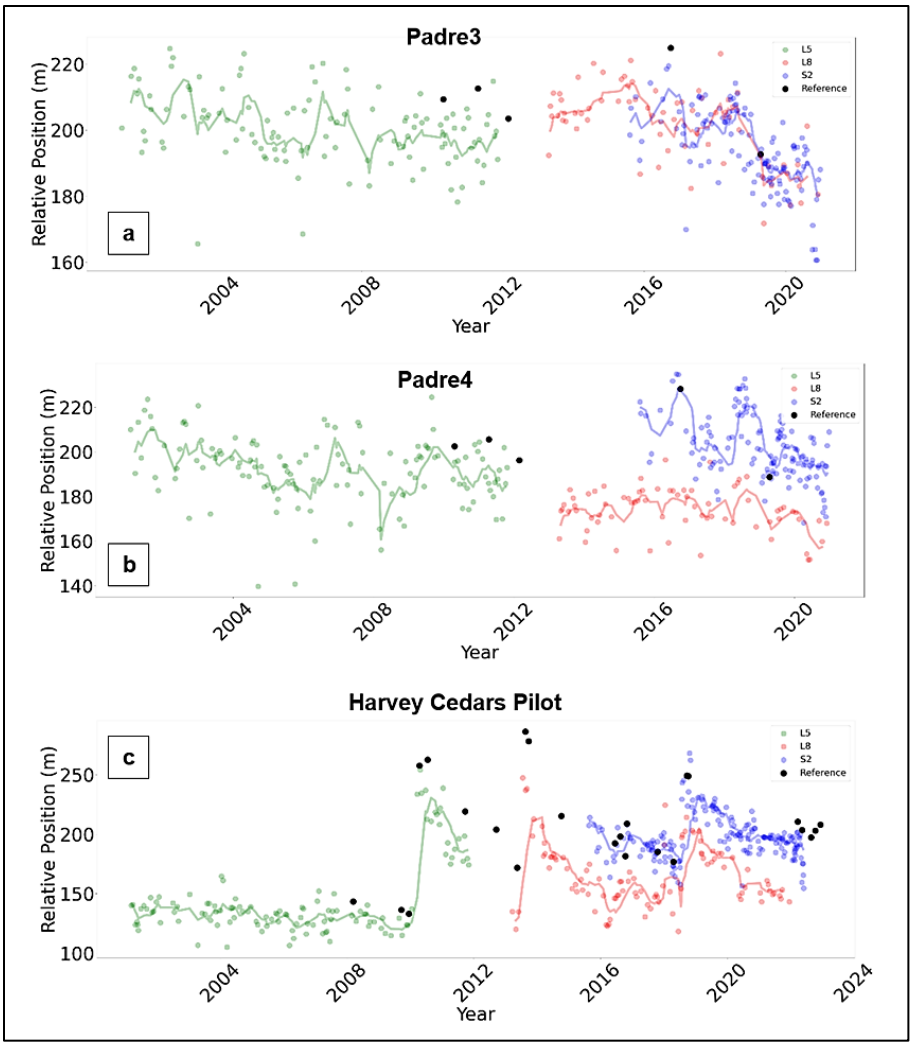

In terms of bias, results show a mean direction of –3.51 m (standard deviation = 12.57 m), indicating a slight onshore bias for the satellite-derived shorelines when compared to survey-derived shorelines. Specifically, 37.5% of sites were biased towards the offshore and 62.5% of sites were biased in the onshore direction.

At Duck, North Carolina, we found a shoreline position RMSE of 8.50 m, which is consistent with Vos et al. (2019) who reported a RMSE of 9.0 m. It should be noted that Vos et al. (2019) conducted comparisons at a single transect and our comparisons extended 1–2 km in the alongshore, depending on the length of the FRF survey at specific times. Figure 14 provides visual examples of low and high shoreline position accuracy time

intervals at Duck. An example of the consistent landward shoreline bias at Duck is evident in Figure 14 (*right* panel) where a mean horizontal difference from ground truth in shoreline position of 21.1 m is visible.

Figure 14. Examples of high- and low-accuracy satellite shorelines relative to ground truth surveys at Duck. Note the crossing shorelines in the *left* panel.

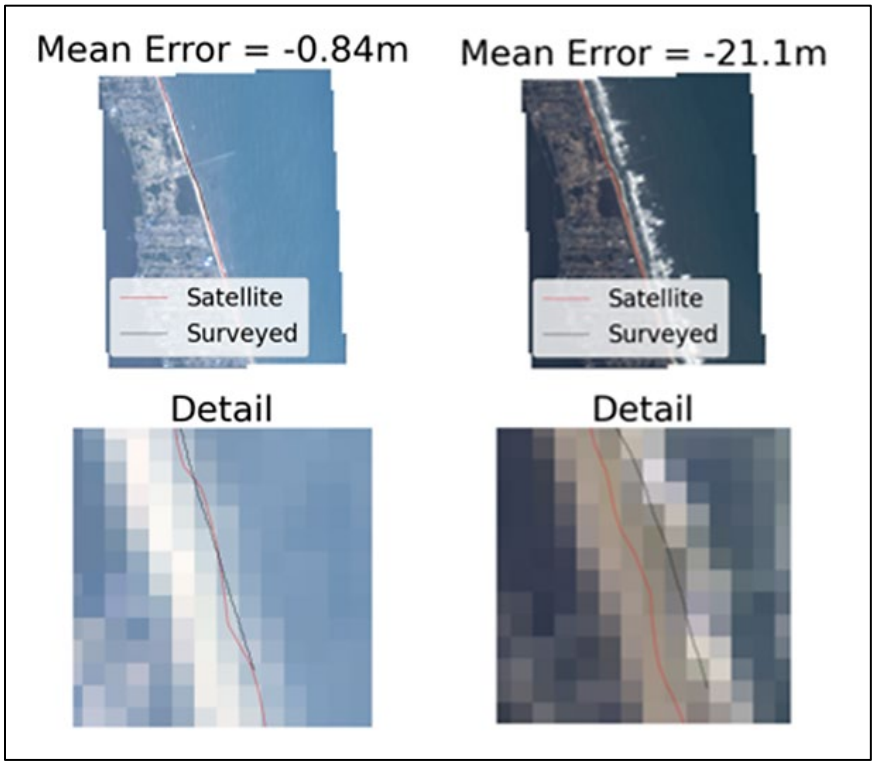

4.1 Satellite Mission Comparisons

Since CoastSat ingests Landsat and Sentinel imagery, we examined each satellite mission separately for accuracy and bias for all sites. Each satellite mission shows a different bias where negative values indicate shoreward direction bias and positive values reflect seaward bias (L5 = −6.93 m, L8 = −1.21 m, S2 = 1.90 m)(Figure 15). The mean horizontal difference from the reference shorelines was L5 = 10.52 m, L8 = 10.57 m, S2 = 8.86 m (Figure 15). With each generation of satellite, bias and mean horizontal difference decrease. Landsat 5 and 8 have a mean horizontal difference that is 53 and 58% lower than the native short-wave infrared (SWIR) resolution of 30 m, respectively. The mean horizontal difference for Sentinel 2 is 41% lower than its SWIR resolution of 20 m.

Figure 15. Mean horizontal differences in satellite shorelines from ground truth for different satellite missions. Negative values represent the landward direction, and positive values are seaward relative to ground truth surveys. The absolute shoreline offset panels disregard the directional biases.

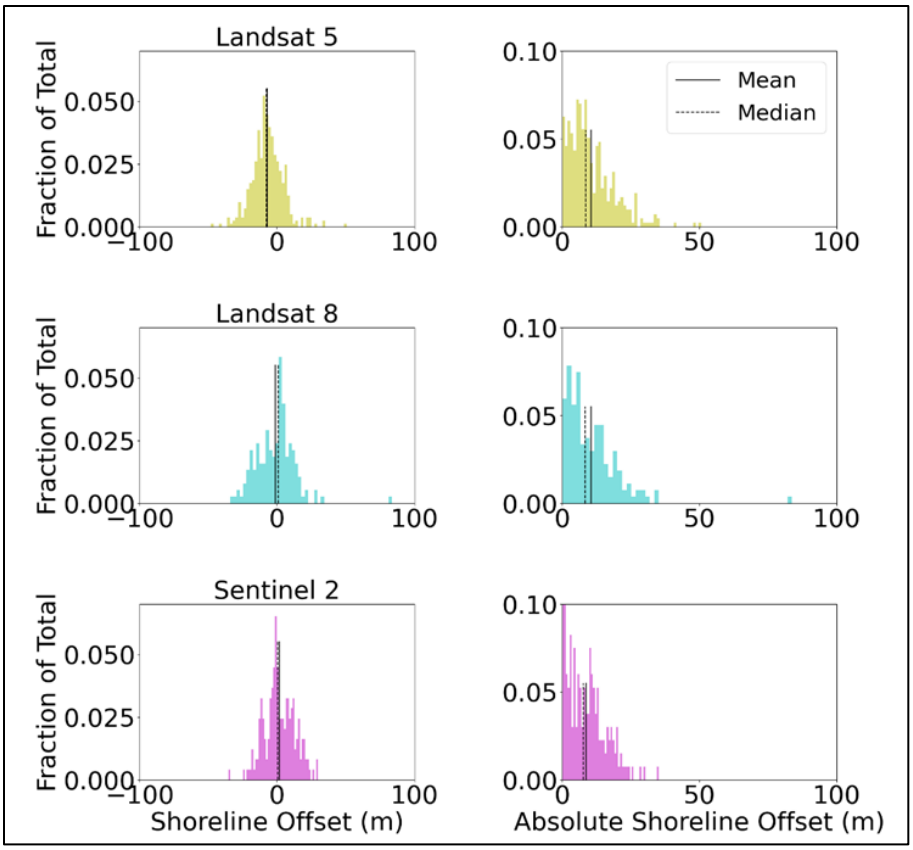

4.2 Image Coregistration

One of the major challenges of using satellite images to track environmental conditions through time is the imprecise georeferencing accuracy for the images themselves in addition to the differences in georeferencing accuracies when using multisensor data sets. While Landsat 7 has a reported image registration accuracy (linear error with 90% confidence; LE90) of 12.0 m (Storey et al. 2014) and Sentinel-2 has a reported image registration accuracy of 12.5 m (Trémas et al. 2015), Storey et al. (2016) estimate that the sensor data can be misaligned by 38 m. One of the challenges involved in coregistering the images is the quantity and spatial extent of images used in remote sensing applications such as this, causing it to be temporally and computationally expensive (Scheffler et al. 2017).

There are multiple strategies when aligning imagery which can be simplified into two main groups—intensity-based and feature-based.

Intensity-based techniques rely on similar patterns of grey values in the image, while feature-based processes look for specific identifiable objects. Feature-based processes tend to be less computationally and temporally expensive, but require features to be evenly distributed throughout the image which can be difficult to rely on in coastal environments. Because of this, applying intensity-based processes to the imagery was investigated in this study. Intensity-based processes are more computationally expensive, but do not rely on distinguishable features and can achieve subpixel shifts (Scheffler et al. 2017; Tondewad et al. 2020).

Two coregistration tools were investigated using satellite images of Wrightsville Beach, North Carolina, Automated and Robust Open-Source Image Co-registration Software (AROSICS) and the ArcPy georeferencing tool. Wrightsville Beach was not included in the statistics of the report, but it is an area of interest as it lies just east of the Wilmington District. AROSICS for multisensor satellite data, is an intensity-based registration technique using phase correlation. While this tool is open-source and python-based, multiple problems arose when trying to integrate this tool into the CoastSat workflow. It is anticipated that the imagery format, as downloaded from GEE and different per mission, caused difficulties when using AROSICS to coregister the whole data set together. Instead, images could only be registered to its same missions' baseline. In theory, this would still perpetuate the known offsets between missions (38 m). There are two functions in the AROSICS package, *COREG* and *COREG_LOCAL*. *COREG* applies a global *X*/*Y* translational shift to the image, whereas *COREG_LOCAL* creates a dense grid of tie points, filters the tie points for false positives, and uses the valid tie points to fine-tune the parameters in an affine transformation. A cubic resampling technique is applied to finally warp the image. Because spatial offsets between images are highly varying, *COREG_LOCAL* was applied to the imagery. This process was very computationally expensive and would require many hours to complete the whole Sentinnel-2 data set for Wrightsville Beach (91 images). Additionally, the subsequent efforts to map the shoreline from the coregistered image using CoastSat were unsuccessful. We believe this is because the SWIR band was not coregistered along with the RGB bands. This would cause the supervised classification to resemble the coregistered image, but the MNDWI would have artifacts resembling the original image. This prompted investigation of other methods to coregister the data set.

ArcPy was a much simpler tool to integrate into the workflow and was much faster, on the scale of minutes (about 0.5 s an image for a total of 45.5 s for the 91 images) versus hours to coregister all of Sentinel-2 images in the test site to a base image with low initial registration error as evident in the metadata. ArcPy generates tie points (Figure 16) from an intensity-based approach and then fits a first-order polynomial transform to warp the image (Figure 17). The difference between the raw and coregistered, an example of which is shown in Figure 17*C*, was typically subtle and can be detected mostly in shifts of bright infrastructure. Because Sentinel-2 has worse georeferencing and to save time for the end user, this process was applied to just the Sentinel-2 images from the test site to investigate the effect it had on the shoreline positions mapped using the CoastSat algorithm (Figure 18).

As shown in Figure 18, in the northern portion of transect 1140, the mean position was shifted landward (down) from the raw shorelines (*dark blue*) to the coregistered shorelines (*light purple*).The detrended standard deviation for transect 1140, a proxy for noisiness, was reduced from 9.90 m to 8.99 m after coregistration. In addition, the shoreline change rate changed from –4.6 m per year to –4.4 m per year. The southern transect (transect 1030) shows a similar change in mean shoreline position and noisiness. The detrended standard deviation for transect 1030 was reduced from 12.17 m to 9.99 m after coregistration. The shoreline change rate at transect 1030 changed from –1.88 m per year to –0.56 m per year. As shown in these two transects along Wrightsville Beach, if appropriate tie points are picked, the spread of shorelines could be reduced, thus decreasing the noise of the satellite-derived shoreline positions and potentially leading to lower RMSE and a better depiction of historical shoreline movement.

Figure 16. Wrightsville Beach image with tie points shown in *red* and *green B*'s.

Figure 17. An unregistered image of Wrightsville Beach (*A*), a coregistered image of Wrightsville Beach using ArcPy (*B*), and the difference in the two images scaled to a factor of ten (*C*).

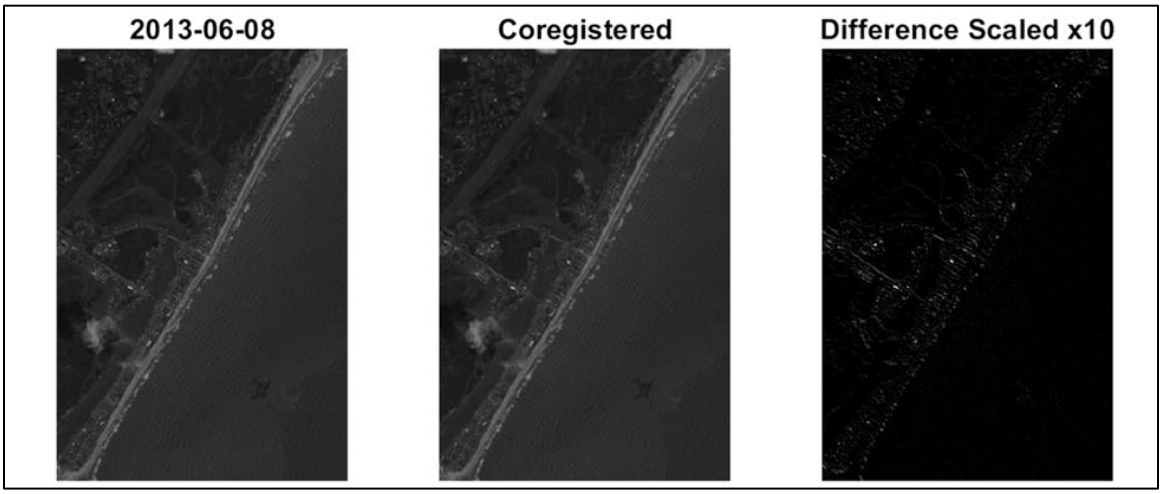

Figure 18. Wrightsville Beach with the cross-shore transects used to analyze shoreline change (*left*); shoreline positions from unregistered and coregistered imagery at transect 1140 and their respective trends (*top right*) and; shoreline positions from unregistered and coregistered imagery at transect 1030 and their respective trends (*bottom right*).

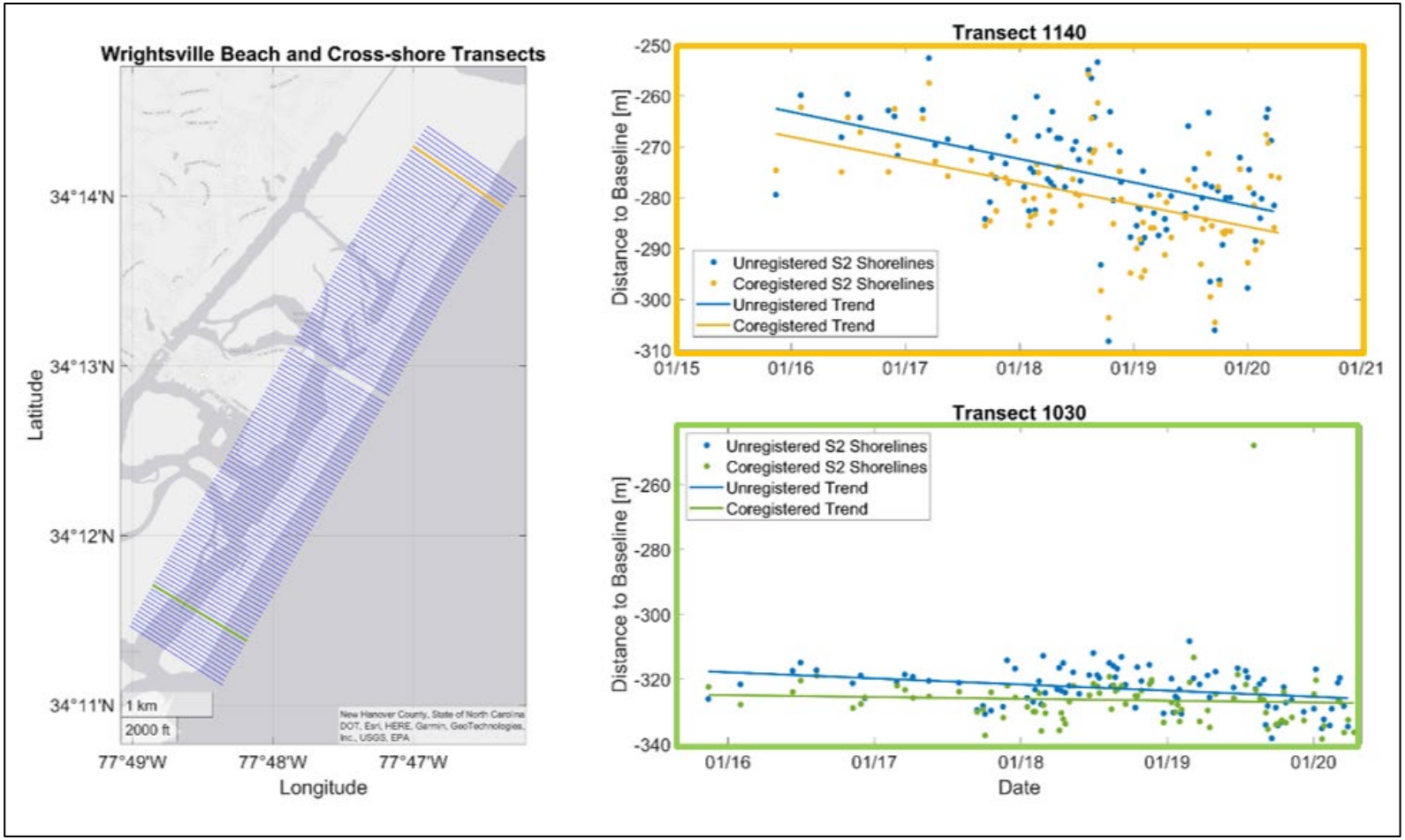

After seeing a reduced spread of shorelines, the same process was applied to the Duck Sentinel-2 images. Unlike Wrightsville Beach, Duck has an ample amount of ground-truth data that we can compare to our coregistered shorelines quantitatively. Using the ArcPy newly coregistered S2 images (n = 548), the associated mean horizontal difference in satellite-derived shorelines compared to ground truth only improved by 6 cm. This minimal improvement in accuracy suggests mission to mission (e.g., Landsat-8 versus Sentinel-2) coregistration may be more critical than intra-mission, though more tests are needed at additional sites with good ground-truth data. Furthermore, if the seed or base image used for coregistration has high georeferencing error, matching other images to the base image may even increase overall errors. Thus, it is critical to ensure your baseline image has high-accuracy. While it is not practical within the current AROSICS or ArcPy framework, a potential improvement may be using a high-resolution base image to register other imagery with, such as UAV image or higher resolution satellite image (e.g., PlanetScope).

4.3 CoastSat-generated Slopes

To correct visually identified shorelines to a consistent datum-based shoreline, the tide level and slope are used in CoastSat. Beach face slope is a fundamental parameter for coastal research related to shoreline change, runup and flooding, yet it often varies through time and is difficult to quantify without conventional field observations. Vos et al. (2020) added the automated capability to extract slopes from historic satellite imagery through the *CoastSat.Slope* toolbox. Vos et al. (2020) found good agreement (R^2 = 0.93) with the approach compared to field observations at eight sites across the globe.

We tested the *CoastSat.Slope* function at the district test sites and compared the output to field survey slopes, where robust slope data were available. It is important to note that even field-based surveys are only capturing slopes at one point in time and, in reality, slopes are likely time varying. Figure 19 shows the comparison of CoastSat-derived versus user input slopes (i.e., measured) with poor agreement (R^2 = 0.24) for the test sites.

Figure 19. CoastSat-generated slopes versus user-selected slopes.

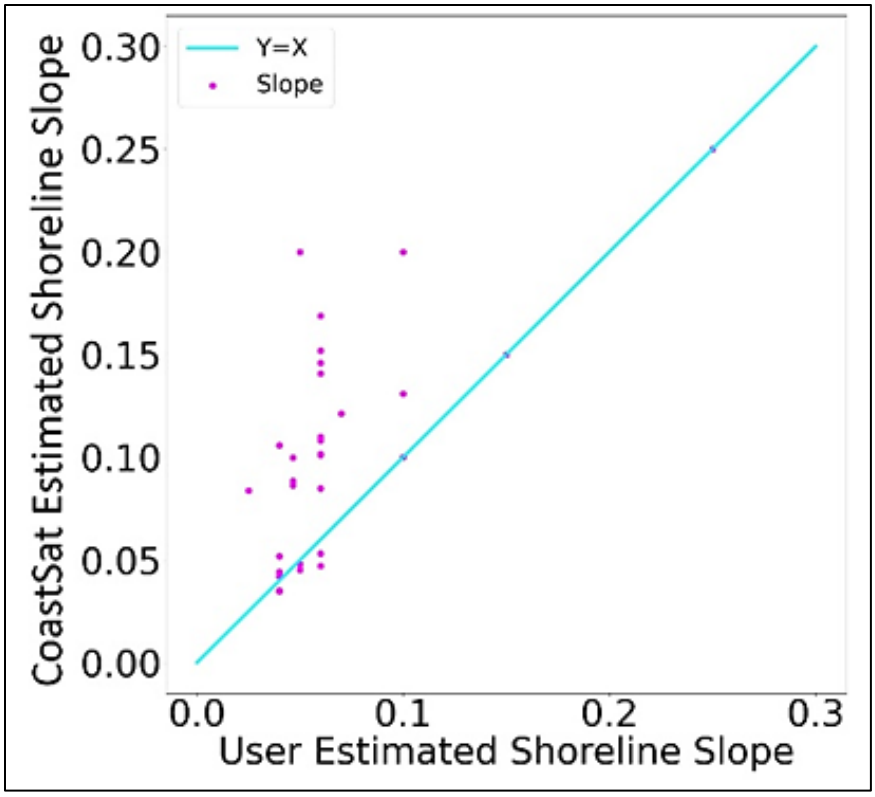

To investigate how slope influences shoreline accuracies, results using the CoastSat-derived slopes were compared to results using the field-measured slope (Figure 20). Using CoastSat derived slopes caused slightly higher errors at 59% of our study sites; however, overall the horizontal differences in satellite versus ground truth shorelines was minimal (0.24 m) when compared across all sites (Figure 20). Considering these results, at most sites, especially where conventional slope data are unavailable, the CoastSat slope function can be reliably used for shoreline extraction, despite its likely poor representation of true slope, which suggests at least at the sites tested here, slope does not exert a strong control on shoreline position accuracy. Notably, Vos et al. (2019) found no significant improvement of shoreline accuracy by using time-varying slopes instead of a time-averaged slope at Narabeen, Australia. Furthermore, at the same site using *CoastSat.PlanetScope*, Doherty et al. (2022) found using time-varying beach slope decreased shoreline position accuracy.

Figure 20. Summary of shoreline offsets for CoastSat-generated slopes (*blue*) and user-selected slopes (*red*).

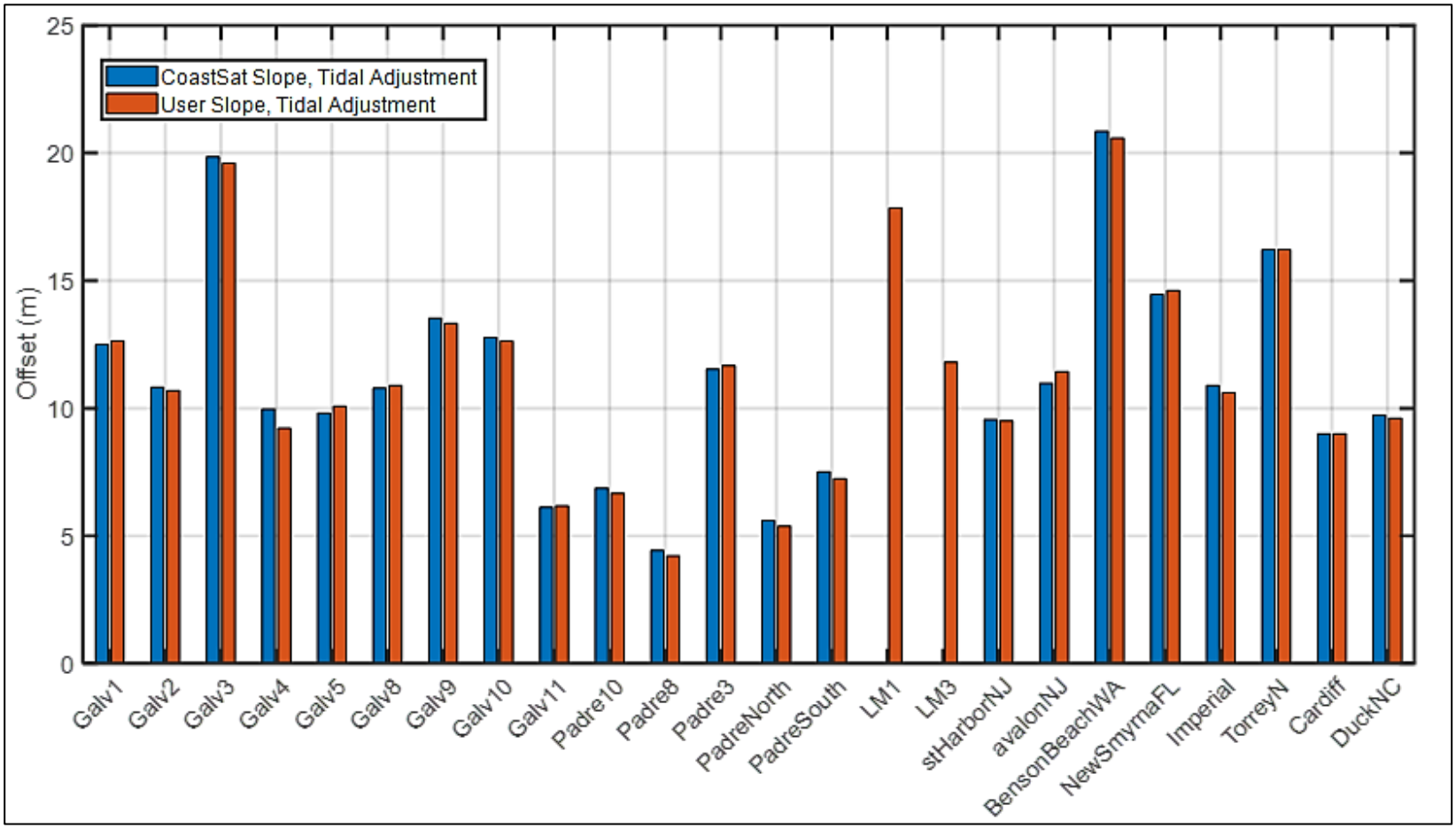

4.4 Tidal Correction Influences

Shoreline position also fluctuates depending on the tidal stage. We assessed the influence of the tidal correction on shoreline positional accuracy in part because some users may be located in areas that do not have hydrodynamically proximal water level gages or predictions. Also, if the tidal correction only provides minimal shoreline accuracy improvement, users could opt to forego the tidal correction step.

For context, the study sites spanned a tidal range between 0.74 m and 3.10 m. And for clarification, the Great Lakes sites have no tides so the tidal corrections were not evaluated. Overall, the tidal correction lowered the mean shoreline position error at 82% of the sites (Figures 21 and 22) with a reduction of –1.24 m in mean horizontal difference between satellite and ground truth shorelines. The largest accuracy improvements from tidal corrections for mesotidal sites were Avalon, New Jersey (–4.22 m), Stone Harbor, New Jersey (–2.75 m), and Cardiff, California (–2.71 m); the microtidal improvement was Galveston, Texas (–3.36 m); and the macrotidal improvement was Benson Beach, Washington (2.32 m).

Across sites for all reference times the mean horizontal difference was 12.45 m without the use of tidal correction (Figure 21). When tides were corrected with the built-in *CoastSat.Slope* function to determine the beach slope along which to shift the shoreline, the mean horizontal difference was reduced 11.0% to 11.08 m. With the inclusion of a user given slope, determined by ground truth data and associated reports, the mean horizontal difference is reduced to 11.21 m. With the use of user estimated slopes and tidal correction sites varied from 4.2 m to 20.6 m of horizontal difference between the satellite derived shorelines and the reference data.

It is important to note that finding an open coast tidal station that is hydrodynamically proximal to your study site is crucial for proper tidal correction. We initially used an automated approach to select simply the closest tidal stations to each site; however, several of those selections were in inlets, bays or inshore which resulted in high shoreline position errors since the timing and magnitude of the tidal correction in those areas are not reflective of the open coast.

Figure 21. Bar plot showing satellite shoreline position accuracies without any tidal correction (*blue*), with a tidal correction using CoastSat slopes and tidal correction with user slopes.

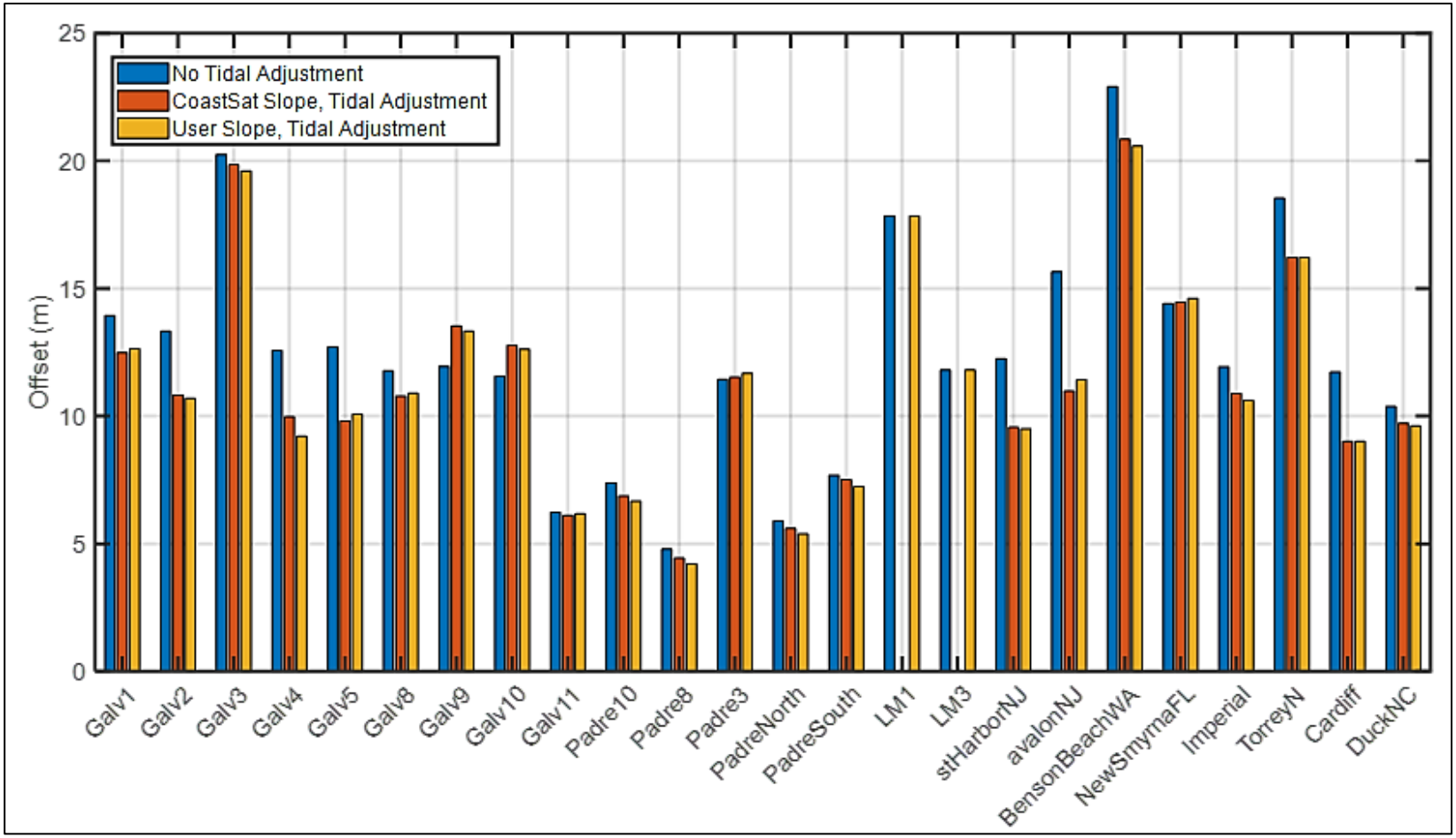

Figure 22. Impact of tidal corrections where *gray* positive values reflect the amount of improvement in meters after a tidal correction. *Reds* represent instances where tidal correction decreased accuracy.

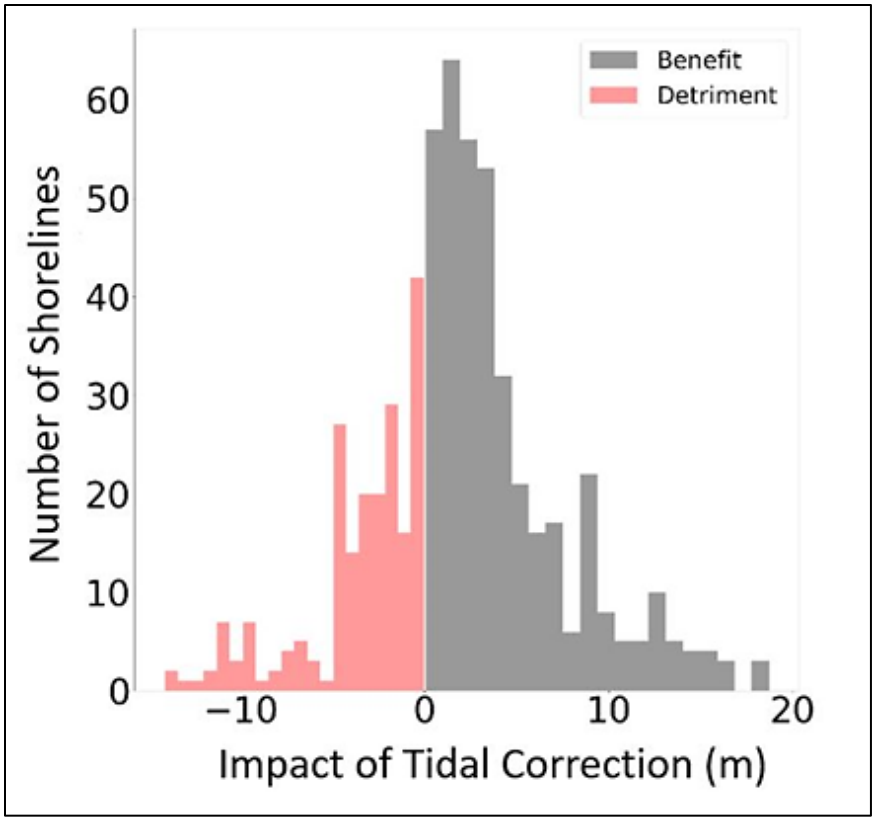

We also examined shoreline accuracies relative to different tidal ranges. When the tidal range is combined with the site slope to calculate a horizontal distance, or horizontal tidal envelope, there appears to be a weak correlation with satellite shoreline accuracy, where generally larger horizontal tidal envelopes have higher shoreline position error (Figure 23). Furthermore, Figure 23 highlights the general trend in slightly lower shoreline errors associated with user versus CoastSat slopes.

Last, we assessed shoreline positional error relative to tidal range and satellite mission. Figure 24 shows no apparent link with these parameters. Coincidentally, Landsat 5 encompassed the majority of our comparisons of satellite-derived shorelines and ground truth surveys at lower tide range sites (Figure 24).

Figure 23. Shoreline offset versus horizontal tidal range generated from CoastSat slopes (*red*) and user slopes (*blue*).

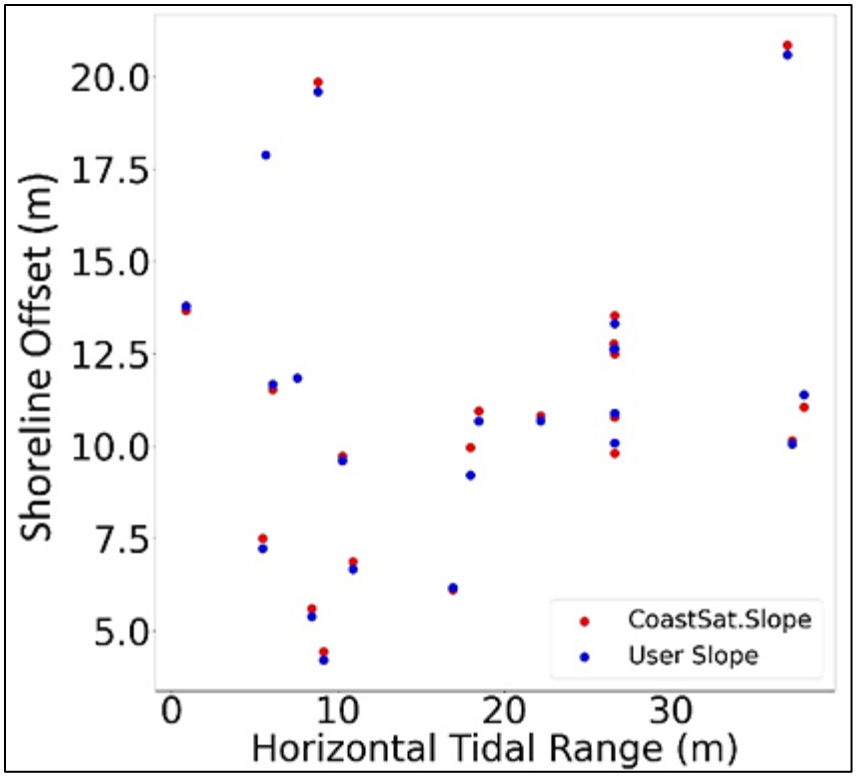

Figure 24. Shoreline offsets across all sites relative to tidal range and satellite missions.

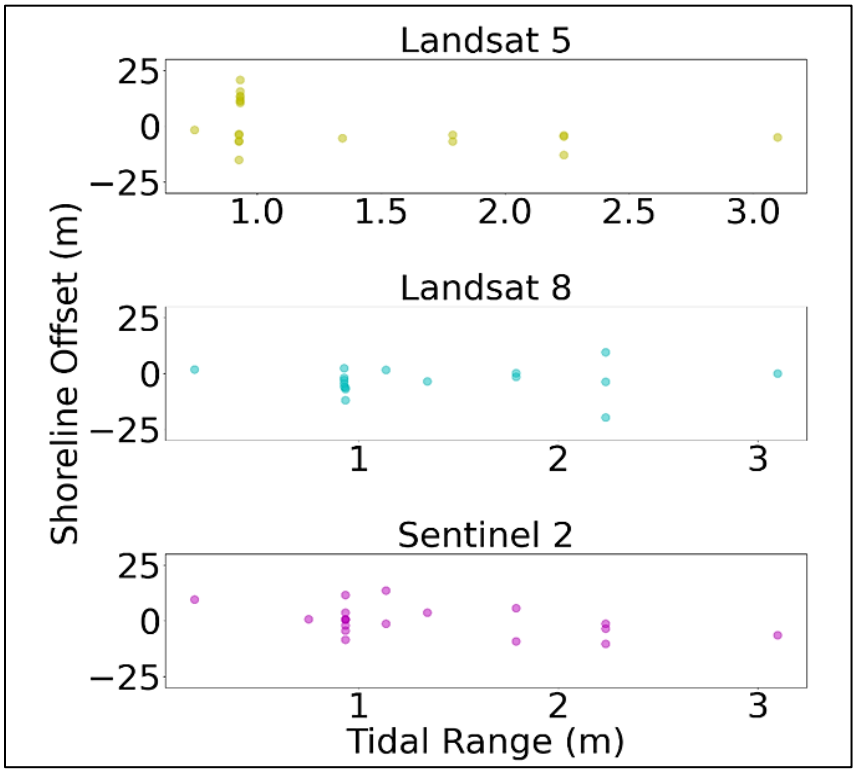

4.5 Wave Runup Corrections

While CoastSat incorporates tidal corrections based on image capture time, it does not account for wave processes and high frequency swash motions (i.e., setup, runup, rundown, and infragravity). An instantaneous satellite snapshot may occur during wave runup or rundown, yet this is not known, thereby leading to challenges in integrating a wave correction. Furthermore, wave and swash processes generally vary alongshore, adding even more complexity (e.g., Stockdon et al. 2007). To address these concerns, we focused on five sites with robust available wave data and frequent reference data—Duck, Benson Beach, Cardiff, Imperial, and Torrey Pines North.

Likely due to the high frequency of swash motions, results showed adding adjustments for runup improved shoreline accuracy at 60% of the sites (Figures 25 and 26). We suspect that this is in part due to the randomness of waves relative to image capture time. Also, adding wave runup offsets effectively can only shift a shoreline more seaward, so if it was already too far seaward, runup would exacerbate the shoreline position accuracy. Figure 26 shows that when combining the site slope with runup to create a runup envelope, roughly half of ground truth comparisons improve in terms of accuracy and the other half have higher shoreline offsets. Future work could explore creating a shoreline position envelope based on the equation,

$$\text{Tide elevation} + \text{setup} \pm \frac{S}{2}, \tag{3}$$

where S is the significant swash height from Stockdon et al. 2006, for example. Satellite shorelines could then be assigned a potential water-level related uncertainty and considered accurate if surveyed shorelines fell within this envelope.

Figure 25. Results of runup corrections at five test sites. *Red* indicates user slope with no runup correction, *green* is user slope with runup correction, *blue* is CoastSat slope with no runup correction, and *light blue* is CoastSat slope with runup correction.

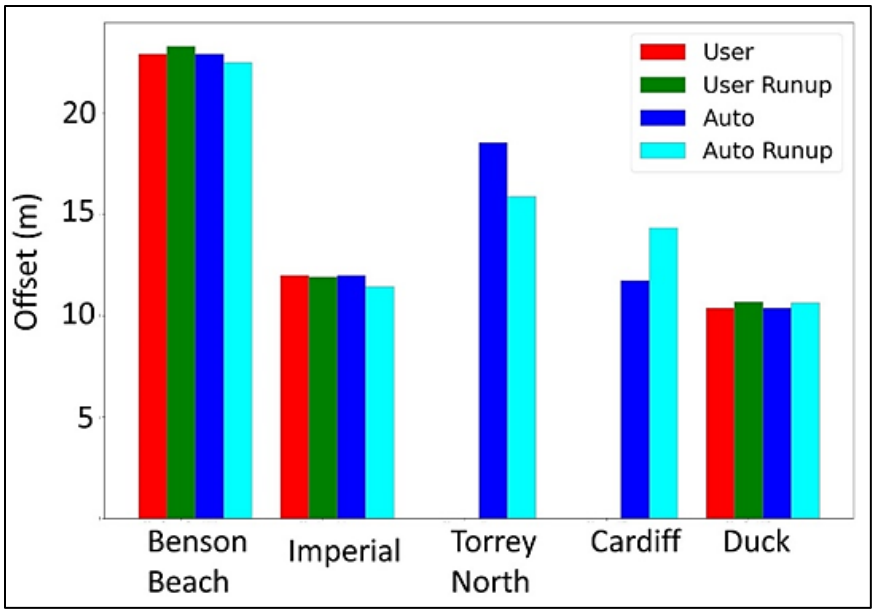

Figure 26. Shoreline offsets (meters) for all runup test sites versus horizontal wave runup envelopes (meters).

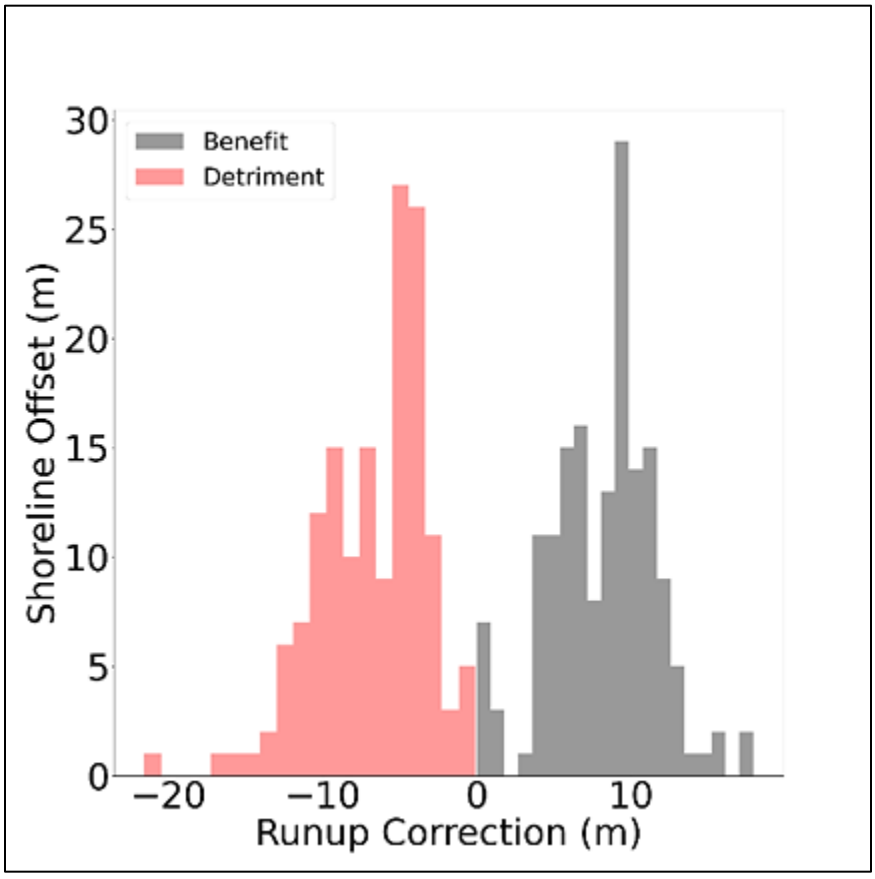

We also evaluated runup corrections during different seasons (Figure 27) and wave conditions (Figure 28). Figure 27 shows some weak correlation between seasons and shoreline accuracy where the better accuracies are found during summer months and the lower accuracies are during the stormier winter season. Based partly off seasonal trends and results of Figure 28, we considered implementing runup corrections only during stormy intervals, yet determining a specific wave height threshold is also challenging and would likely need to vary site by site. At Duck, for example, implementing runup correction only when waves were >1.5 m, caused overall improvement of 0.5 m (9.6 m to 9.1 m) in mean horizontal difference between ground truth and satellite shorelines. Yet, Figure 28 shows there is no clear link of shoreline accuracy improvements from wave corrections in high and low wave conditions at other sites.

Past work aimed at reducing noise in swash motions has used composite images averaged over long time intervals or elevation correction models (Almeida et al. 2021; Bishop-Taylor et al. 2021; Luijendijk et al. 2018). Castelle et al. (2021) used CoastSat at Truc Vert, France and applied an elevation correction model which was successful in reducing satellite-derived shoreline position error by half. However, this is in part attributed to the slope (0.05), interannual variability in waves (Hs of 1.1 m in summer and Hs of 2.4 m in winter), and meso-macrotidal regime (tidal range up to 5 m) which make runup effects more pronounced at this site. On the contrary, using CoastSat with PlanetScope imagery (3 m resolution) at Narabeen-Collaroy, Australia and Duck, North Carolina, Doherty et al. (2022) found implementing time varying runup only caused negligible improvements on satellite-derived shoreline accuracy (<1%). Doherty et al. (2022) suspect the results are due to the steeper nature of the coastline (average intertidal slope of 0.09), less interannual wave variability and microtidal regime (mean spring tidal range of 1.3 m), that make the shoreline less susceptible to large horizontal movements of swash motions.

More research is still needed to determine whether these cases of runup correction are site specific. Not having to account for wave processes would be advantageous since nearshore, high resolution wave data may not be available or difficult to obtain in many locations.

Figure 27. Average monthly shoreline offset (meters) across five runup correction test sites.

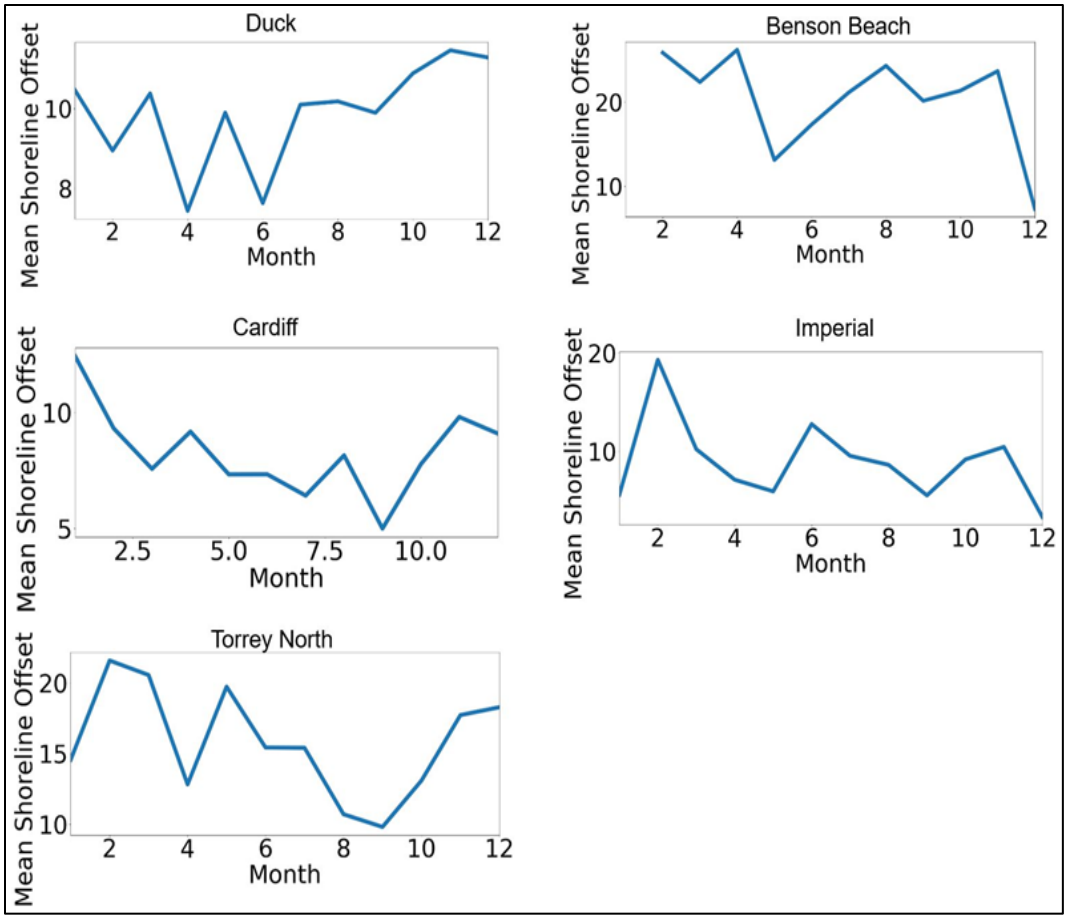

Figure 28. Summary for runup corrections at all five sites where the y-axis is mean shoreline satellite position error and x-axis is wave height. The *dot* and *arrow* combinations show the magnitude of error increase (*red*) and decrease (*black*) where the dot represents the initial shoreline error prior to runup correction.

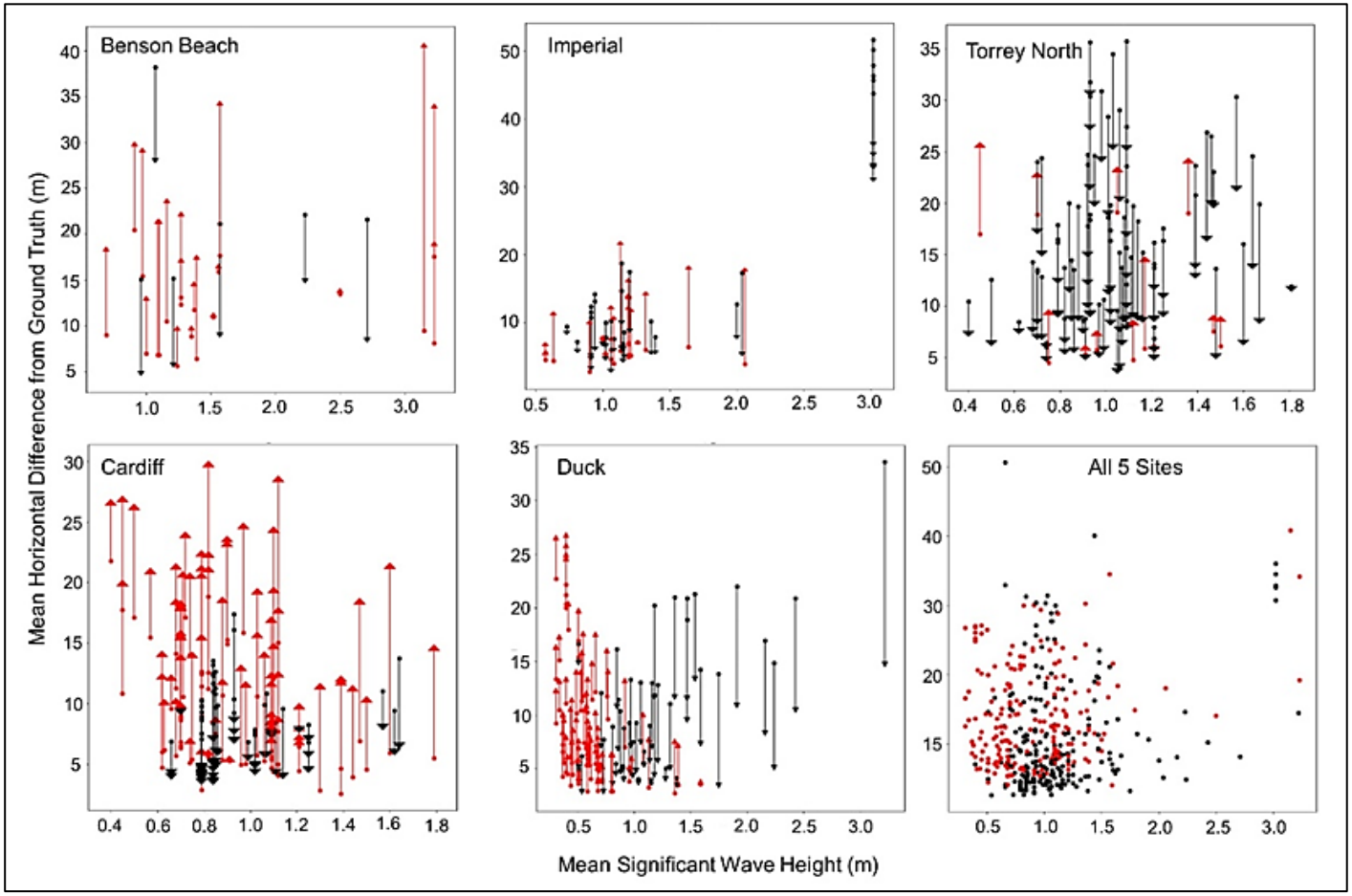

5 Shoreline Trend Comparisons

In this chapter we examine the twenty-year trends derived from satellite imagery and compare them to ground truth data. We first explore how accuracy varies with time, then discuss the trends in more detail at selected sites. Specifically, we address how satellite trend data can be used to monitor subaerial equilibration and evolution of different coastal management strategies and for storm impact and recovery assessments.

5.1 Temporally Variable Confidence

After examining the accuracy of the individual shorelines, the ability to estimate shoreline evolution trends from the timeseries was assessed. To do this, the slope of the shoreline position relative to the transect root as a function of time was assessed for every combination of reference survey times, inclusive of surveys occurring between those pairs. A corresponding set of shorelines was selected from the satellite derived collection spanning the same time period. Figure 29 illustrates this concept where both short and long trends were compared to reference data.

Figure 29. A schematic representing the way in which different time interval trends (*blue*) were examined relative to reference data (*red crosses*).

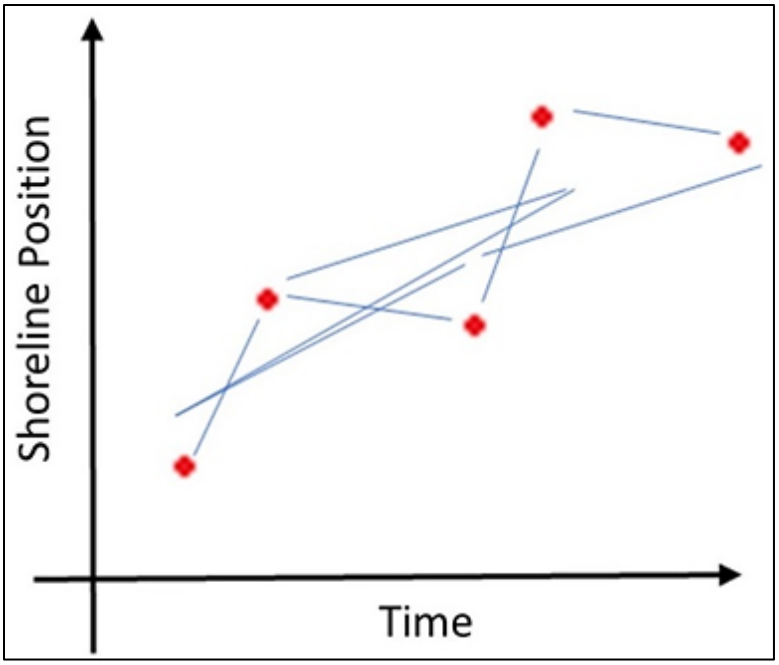

As the number of passes included in the subset of the collection increased, the accuracy of the trend improved rapidly (Figure 30). With a subset encompassing 200 days of data, the mean difference in the trend was 3.10 m/yr, with a standard deviation of 44.07 m/yr (Figure 30). With a subset encompassing 650 days of data, the mean difference in the trend was −0.04 m/yr, with a standard deviation of less than 9.74 m/yr (Figure 30). These trend accuracies related to time may be important to consider for certain users when selecting time intervals. Examples of the shoreline trends and management applications of these data are explored at select sites in the following section. We will show satellite-derived shorelines are able to quantify annual cycles, response to nourishment and storm events, and long term trends, all of which can improve management of coastal resources.

Figure 30. Trend differences (meters/year) of satellite-derived shorelines compared to ground truth shorelines relative to time in (years). The second panel is a zoom of two years.

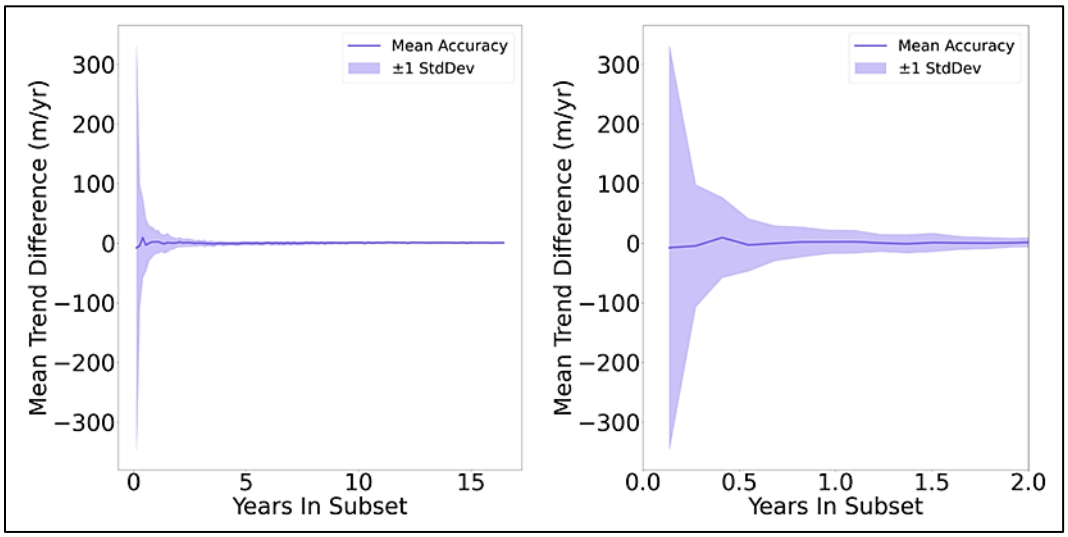

5.2 Harvey Cedars, New Jersey

The Harvey Cedars test site is characterized by a narrow beach from 2000 to 2008 with interannual variability likely driven by seasonality (Figure 31). During this interval, the satellite-derived data show poor alignment with ground truth data with an offset of approximately 25 m, likely due to the GEE mission offset issue. However, post-2010, the data shows good agreement, especially during beach nourishment projects. From the satellite data, we can easily quantify changes to the beach in response to management actions. The first major beach nourishment (2,991,805 yd^3) during the 20-year study period was conducted in 2010, showing a

pronounced increase in beach width on the order of 110 m. After the project was constructed, equilibration was accelerated by Hurricanes Irene (2011) and Sandy (2012). Over a period of 2.8 years, the beach width was reduced by 116.1 m to preproject width, at a high rate of –41.76 m/yr. Following Hurricane Sandy, an emergency repair nourishment was conducted which returned the beach to roughly the 2010 postnourishment width. Shoreline retreat at a rate of 19.35 m/yr followed but the beach remained approximately 20 m wider than the period from 2000–2008. The last nourishment occurred in 2018 and by 2.4 years later had equilibrated to pre-repair beach width (–18.78 m/yr). The satellite-derived shoreline record thus can be used to demonstrate and quantify the impacts of coastal management on the shoreline position. Specifically, that active nourishment and coastal management has resulted in a beach that is on average 20 m wider in the last 10 years when compared with the unnourished beach, even during a period which saw an extreme storm. These data can help communicate the value of active coastal management and enable decision makers to evaluate if the costs are worth the benefits. In addition, the long satellite record can be used during feasibility studies to quantify the background natural variability to the system prior to funded monitoring efforts.

The last, most recent management project at Harvey Cedars was the emplacement of a nearshore berm as beneficial use of dredged material from a federal navigation project in response to an erosional hotspot identified by the Federal CSRM project. In the summer of 2021, 83,300 m^3 was dredged from Barnegat Inlet and placed in the nearshore (2.75 m depth) of Harvey Cedars. Work to analyze the evolution of the placement is ongoing using in situ hydrodynamic sensors and satellite-derived shorelines (McGill et al. 2023). Preliminary results show a lagged widening of the shoreline at the adjacent beach of 5–10 m (Figure 32). These satellite data can potentially reduce the costs associated with monitoring coastal management actions and are capable of capturing the shoreline response from a small scale engineering project.

Figure 31. Twenty-year shoreline trends at Harvey Cedars Pilot site.

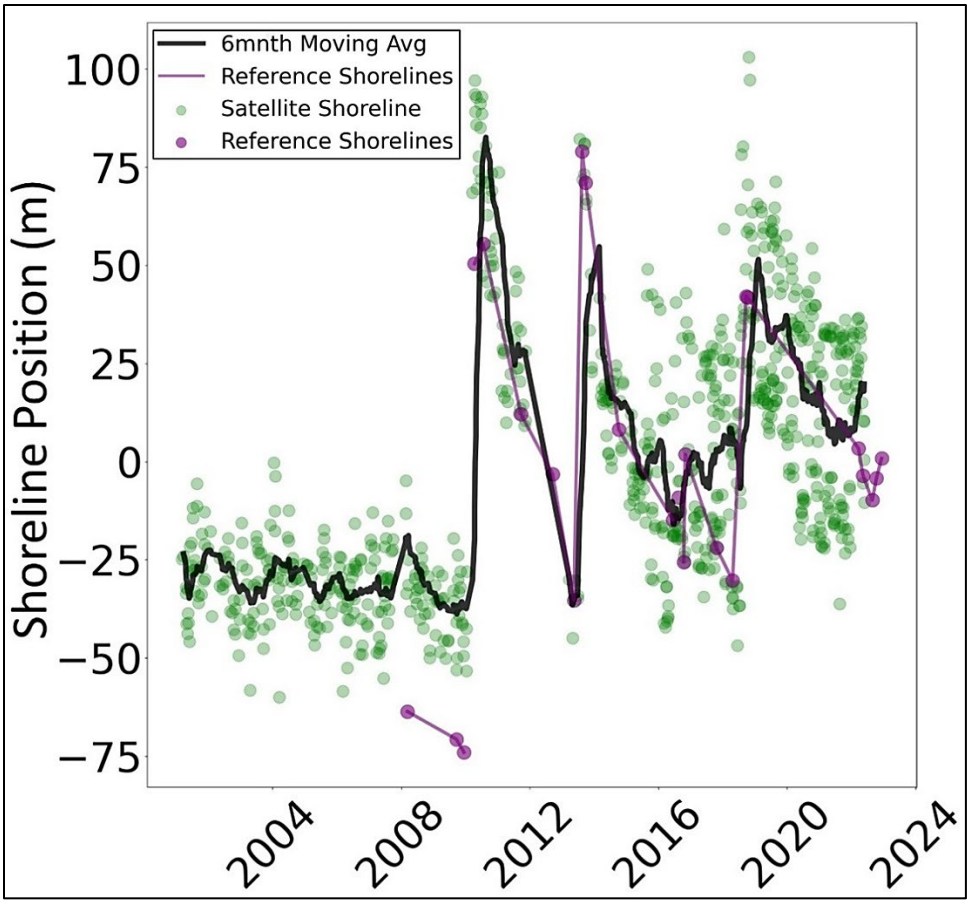

Figure 32. Harvey Cedars satellite shoreline trends within the nearshore berm placement zone (*purple*), below (south) the placement site (*blue*), and above (north) the placement site (*yellow*).

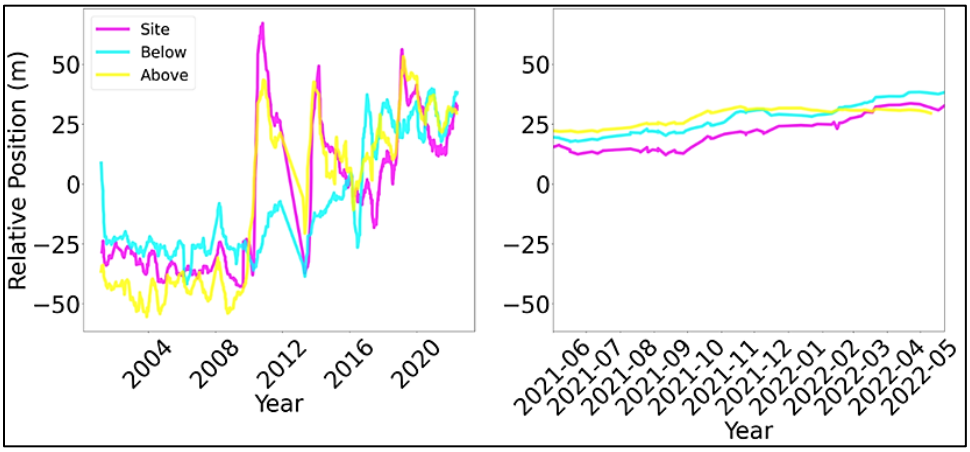

5.3 South Padre Island, Texas

The South Padre Island test site is an example of the paucity of available ground truth survey data to districts. When compared to the five reference shorelines, the satellite derived shoreline positions and trends align well, showing a long-term accretion trend at the site (Figure 33). The satellite data allows for a much more complete depiction of the shoreline evolution at the site. For example, the gap in survey data between 2012 and 2016 fails to capture the interannual and seasonal beach width fluctuations that are on the order of 10 m (Figure 33). In addition, between the last two ground truth shoreline data points, the maximum beach width excursion over the two-decade period is missed.

Figure 33. Twenty-year shoreline trends at South Padre Island, Texas (north).

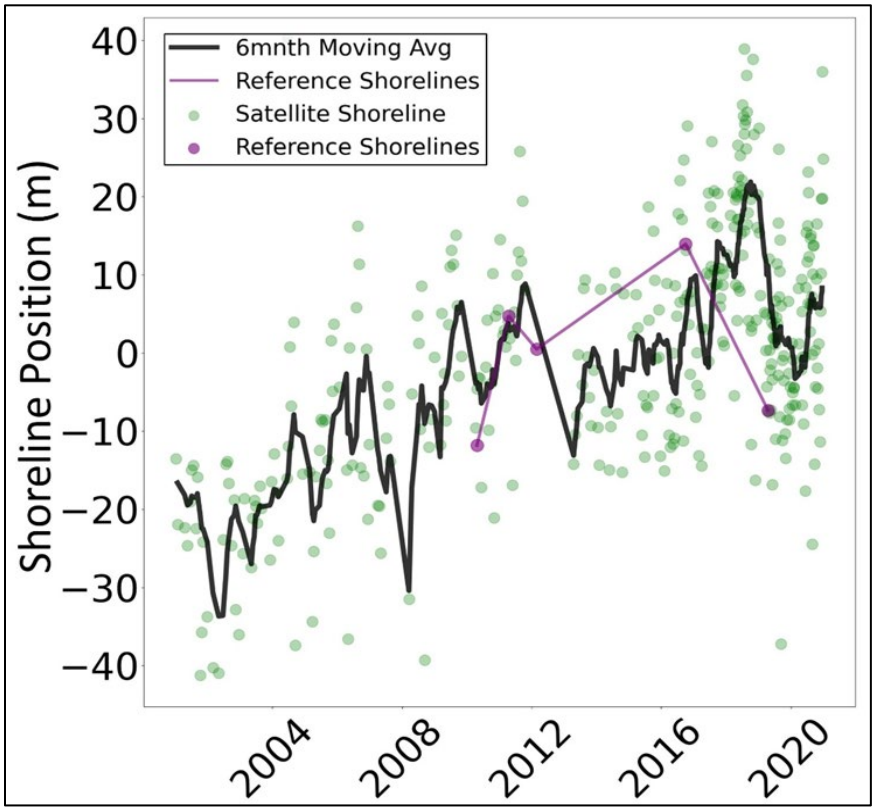

From a coastal engineering and management perspective, the utility of satellite-derived shoreline monitoring is evident. Most nourishments at South Padre Island were small to medium scale (<500,000 yd^3) navigational channel dredging and sediment reuse episodes. The beach width generally increased by 10–20 m following these projects (e.g., Figure 33; peaks in 2005 and 2011). The most recent federal shore protection project nourishment event is also apparent in 2021 with the

increase in beach width on the order of 10–20 m. The strongest storm impacts over this time interval were caused by Hurricane Dolly in 2008, which left a marked erosional signal of approximately 30 m followed by rapid shoreline recovery. Hurricane Hanna in 2020 triggered the notable reduction in beach width (approximately 25 m) as shown by the satellite data. Satellite shorelines can thus be used to inform adaptive management studies by evaluating if assumptions of equilibration rates and recovery intervals from storms within USACE planning tools (e.g., Beach-FX) have been tuned appropriately for a given site.

5.4 Duck, North Carolina

The Duck 20-year trend data shows frequent large changes in beach width, primarily driven by extratropical and tropical storm events. Figure 34 highlights the abundance survey ground truth data, that generally aligns well with the satellite-derived shorelines. Some discrepancies are evident during periods when the survey data show the widest shorelines (e.g., Figure 34; 2003 and 2011). There is also significant noise in the satellite data and examining the six-month moving average line is especially useful for tracking bulk shoreline oscillations (Figure 34; *black line*).

Figure 34. Twenty-year shoreline trends at Duck, North Carolina.

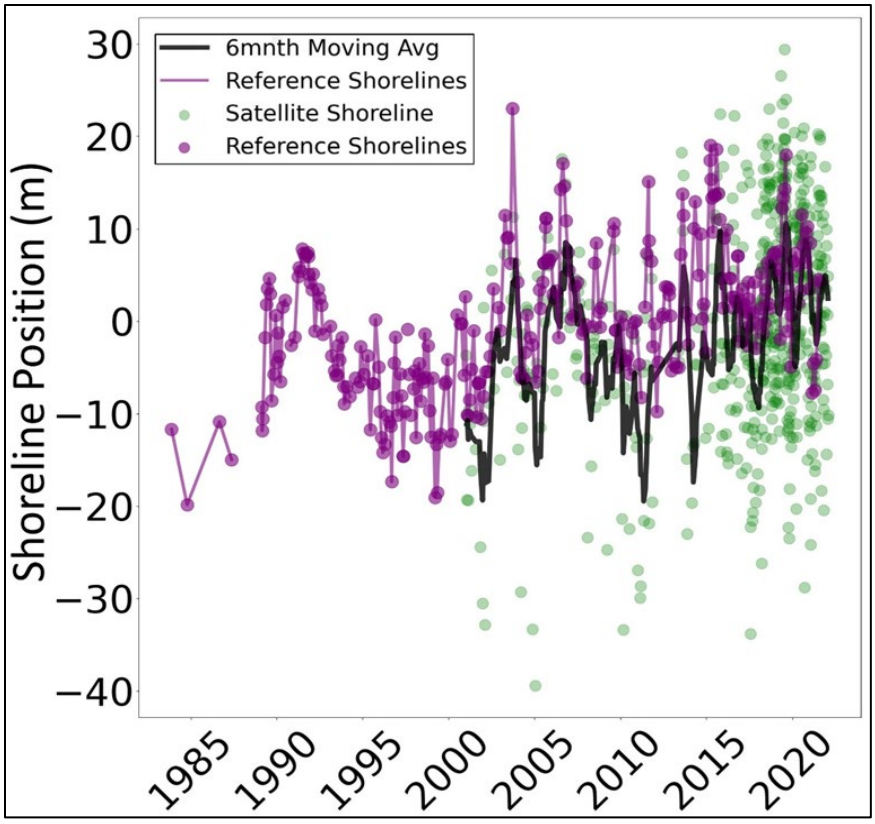

Several storm impact and recovery cycles are clearly shown in satellite-derived shoreline data. For example, Hurricane Dorian in 2019 caused shoreline retreat on the order of 20 m, but one year following the shoreline recovered to prestorm width. The most recent time period is predominantly characterized by severe nor'easter impacts where shorelines receded 10-15 m from storm impacts. These extratropical impacts span long duration stormy periods and often cause more erosion than tropical systems, also noted by Cohn et al. (2022).

The Town of Duck conducted the first beach nourishment project in 2017. To analyze the specific impact of the nourishment, timestacks were created in which the differences in the cross-shore position of the shoreline were normalized by the behavior of the shoreline outside the region of influence of the management action. The timestack (Figure 35) shows the increase in shoreline width following initial construction that started within the monitored area in May 2017. Immediately after construction, alongshore dispersion of the nourishment to the south occurs beyond the nourishment project bounds (also shown in Cohn et al. 2022). Figure 35 shows erosion within the nourished zone beginning approximately 11 months after project construction (Figure 35). Erosion was most severe from late fall nor'easters (Cohn et al. 2022). The large regional extent of the satellite-derived shorelines enabled analysis of the influence of the nourishment to the adjacent coastal areas. The ability to capture temporally dense nourishment evolution, the timing of subaerial equilibration and longshore dispersion rates and diffusion beyond project bounds may be particularly useful to coastal managers and planners designing nourishment projects and developing adaptive management plans.

Figure 35. Satellite shoreline timestack from Duck, North Carolina, where the right y-axis represents the alongshore coordinates (meters) and colors represent shoreline recession (*red*) and advance (*blue*). The differences in cross-shore position of shorelines through time are normalized by the behavior of a shoreline outside the region of influence of the management action. The *black arrow* indicates the start of the 2017 beach nourishment project.

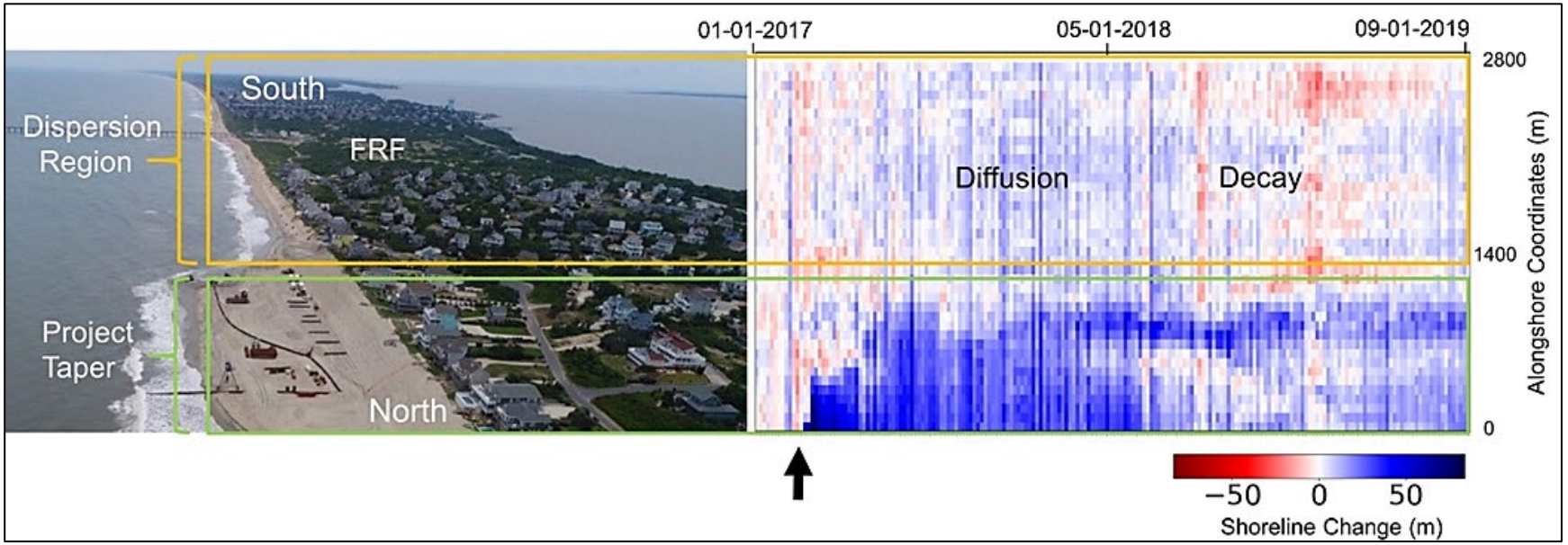

5.5 Avalon, New Jersey

When compared to the ground truth survey data, the satellite-derived shoreline trends show good agreement in Avalon, New Jersey (Figure 36). The periods of time with the widest and narrowest beach widths align well and the satellite imagery is capable of detecting the frequently changing beach widths. If only looking at survey data (*purple dots*) several major shoreline oscillations are missed; for example, there was a large gap in ground truth data from about 2004 to about 2009 which did not capture the shoreline recovery period prior to 2009 (Figure 36). Another example occurs around 2010, where despite more frequent survey data (Figure 36, fourth and fifth *purple points*), a strong erosional perturbation is missed over a short time interval, including observations of when the shoreline was in its most erosive state over the course of two decades.

A gap in satellite imagery does not allow for an assessment of the 2011 nourishment episode, but when examining the two nourishments combined, the beach returned to prenourishment width after 3.6 years, which is roughly equivalent to a shoreline recession rate of 11.9 m/yr. While episodic erosion is missed from Hurricane Sandy (2012) due to lack of imagery, we suspect Hurricane Irene and Sandy were responsible for significant sediment loss during this nourishment cycle (Figure 36). Figure 37 displays the ability of satellite-derived shoreline analysis to capture hurricane impacts, showing an erosional signal of approximately 50 m during Hurricane Irene. This suggests the potential to use satellite imagery in poststorm assessments to quantify impacts to federal project sites and inform applications for emergency relief efforts. The last notable nourishment of 1,636,685 yd^3 was conducted in 2017. Over the next 2.25 years, the beach equilibrated to preproject width, at a recession rate of 23.2 m/yr.

Figure 36. Twenty-year shoreline trends at Avalon, New Jersey.

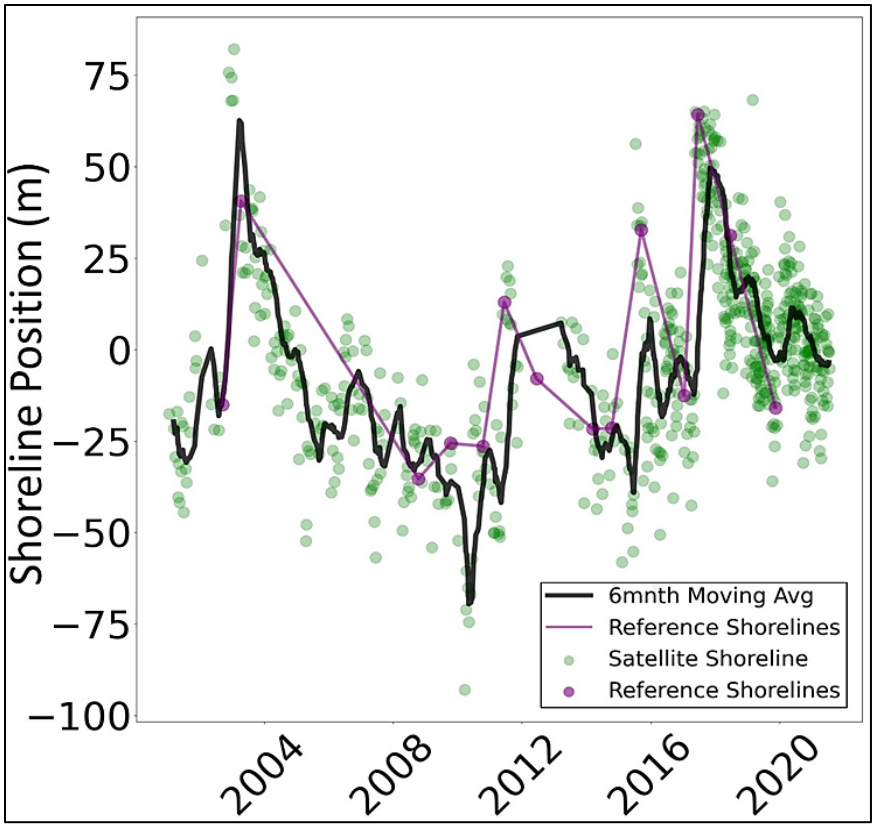

Figure 37. Satellite shorelines spanning from 24 August 2011 to 16 September 2011 with early dates in *blue* and post-Irene (25 August 2011 impact) shorelines in *red*. Note shoreline erosion on the order of approximately 50 m.

5.6 Torrey Pines, California

Shorelines at Torrey Pines, California, exhibit high annual and interannual variability (generally 10–20 m) which the satellite-derived shorelines are capable of capturing (Figure 38). In addition, this site contains cobbles at times which provides an interesting test of the algorithm on an atypical mixed-sediment shoreline. The largest trend discrepancies occur around 2012 when ample usable imagery was lacking.

Figure 38. Twenty-year shoreline trends from Torrey Pines North.

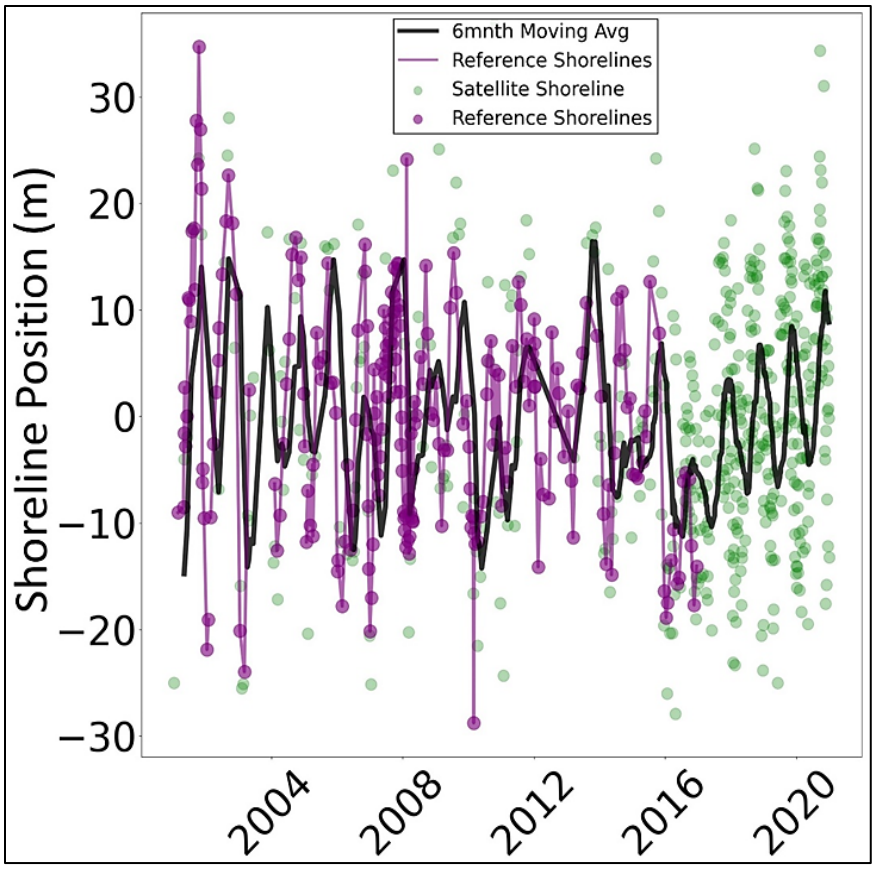

5.7 New Smyrna Beach, Florida

New Smyrna Beach, Florida, presented the opportunity to leverage other coastal imaging work monitoring a nearshore berm placement and to compare satellite-derived shorelines to other visually based digitized shorelines from a mini-argus station (Bruder et al. 2019). This site thus represents a unique example when compared to all other locations, which used 3D topographic data with vertical datum-based shorelines. As noted in the site description, the manual digitization approach to estimating shoreline position has a precision on the order of 10 m and needs to be accounted for accordingly when comparing to satellite-derived shoreline estimates (Onnink 2020). It should be noted that the nature of the shoreline at this site presents challenges in visual delineation because there is a wide saturated zone with dark coloration. Therefore we would expect uncertainty with any visual shoreline approach.

Argus imagery was used to produce timestacks to help assess how the nearshore berm affected the nearshore system and shoreline. As mentioned for Duck, these timesatacks are normalized relative to shorelines outside the area influenced by the management action. The mini-argus timestack is strikingly similar compared to the satellite-derived timestack, emphasizing the utility for monitoring various engineering projects like nearshore berms (Figure 39). Both the mini-argus and satellite derived shorelines show the increase in offshore movement of the shoreline in the lee of the nearshore berm. Also note the additional context provided by the satellite data that extends well before and after the mini-argus deployment. While this is not intended to suggest satellites could replace higher resolution systems like mini-argus that have additional valuable functionality (e.g., timex for wave breaking), it does show the power of publicly available satellite imagery.

Figure 39. Mini-argus–generated shoreline timestack for nearshore berm monitoring (*top*) and satellite-derived shoreline timestack (*bottom*). The *black box* represents the time interval of the mini-argus deployment as reflected in the top panel. Sediment was placed from 1200 m to 1800 m in the alongshore.

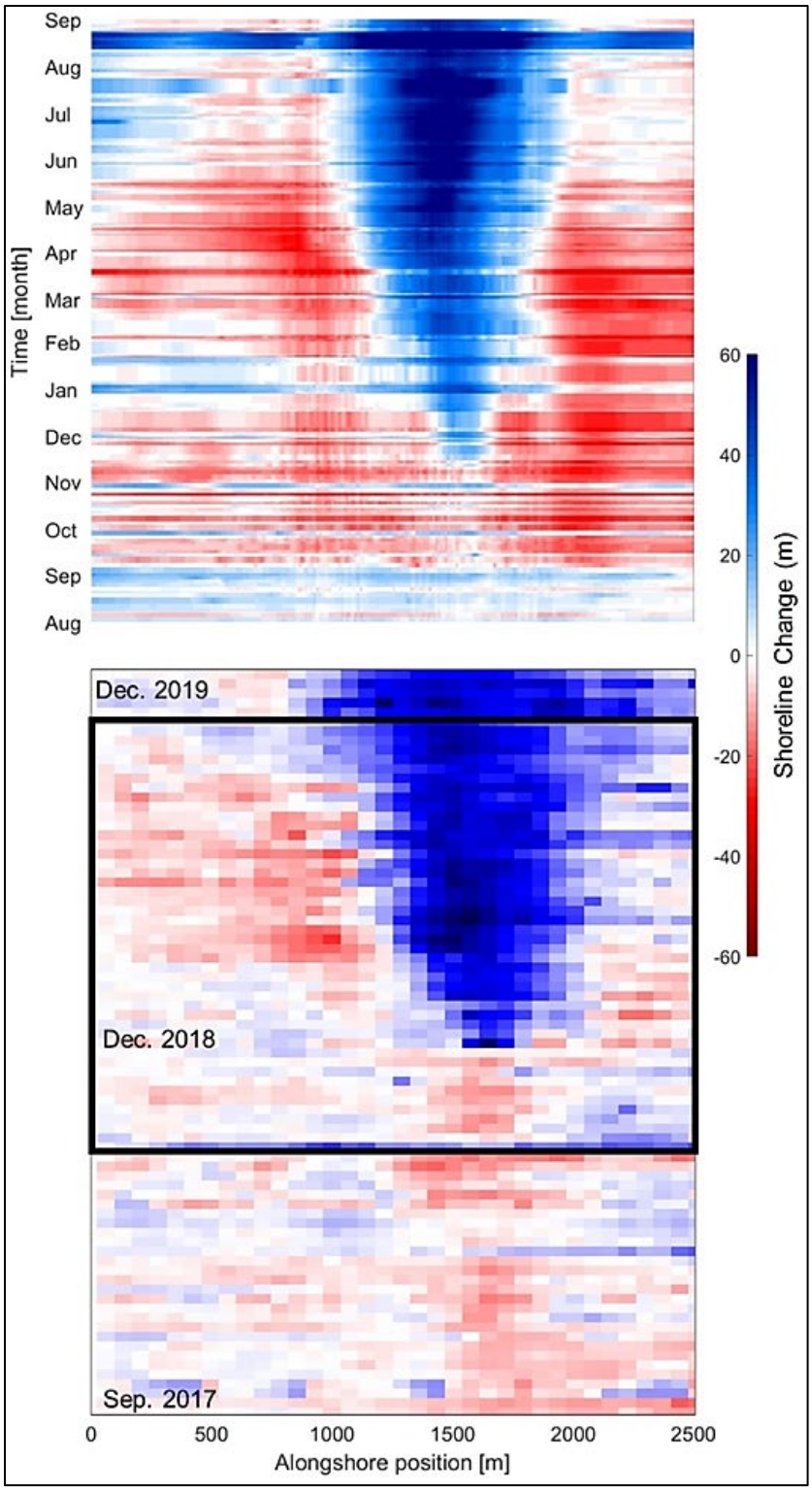

5.8 Wrightsville Beach, North Carolina

While it is not included in earlier analysis, this site was investigated in Brown (2021) and is a good example of frequent large scale federal beach renourishments. Wrightsville Beach received its first nourishment in 1939, completed the first CSRM project in 1965, and was reauthorized in 1986 to continue on a four-year renourishment cycle. These cycles allow for the opportunity to quantitatively evaluate exponential subaerial nourishment decay rates, which may assist with project planning and volume optimization (Figure 40).

Figure 40. Wrightsville beach shoreline evolution from renourishment cycles since 1984. The *colored lines* represent exponential decay of the subaerial beach after each project.

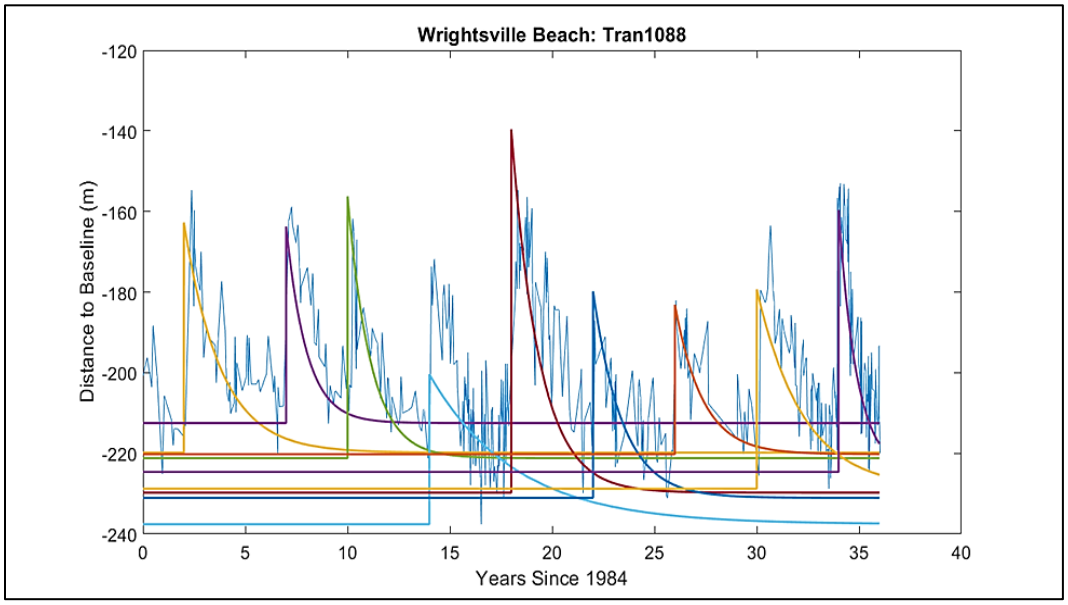

6 Conclusions and Recommendations

6.1 Conclusions

The ERDC research team conducted accuracy testing of the CoastSat algorithm at a total of 37 sites selected across the nation in coordination with district partners. Specific conclusions are as follows:

- Mean alongshore horizontal offsets of satellite-derived shorelines compared to ground truth surveys ranged from 4.2 m to 20.5 m, with an overall mean of 11.32 m and slight onshore bias of –3.51 m. Sentinel-2 was most accurate with a mean alongshore horizontal offset equal to 8.86 m, followed by Landsat-5 (10.52 m) and Landsat-8 (10.57 m).
- Tidal corrections improved accuracies at 82% of our sites. Selection of nearby open coast tidal stations is challenging in some locations, yet it is critical for improving satellite-derived shoreline accuracies.
- While there were some discrepancies in CoastSat-generated slopes compared to user defined slopes, the impact on shoreline accuracy was negligible whereby user-defined slopes improved overall accuracy by 0.24 m. This is advantageous as it shows CoastSat slope function can be used when no field or ground truth derived slope information is available.
- Implementing wave runup corrections slightly improved accuracy at 3 out of 5 test sites where robust wave data were available. Investigation is ongoing to test other runup and setup correction approaches and determine site specific dependencies.
- Twenty-year satellite-derived shoreline trends generally agree well with ground truth shoreline trends. With 200 days of data, the mean difference in the trend was –3.10 m/yr, and with a subset encompassing 650 days of data, the mean difference in the trend was –0.04 m/yr.
- ERDC added several improvements outside the typical CoastSat workflow including more efficient image sorting, tidally shifted shoreline shapefiles, runup corrections and various analysis products.
- Satellite-derived shorelines were able to quantify a variety of impacts from management actions including subaerial beach nourishment equilibration, diffusion and decay, shoreline response to small nearshore berm placements, and background and natural versus engineered shoreline variability. In addition, CoastSat captured many storm impacts and recovery cycles.

- This satellite-derived shoreline approach represents a free and powerful data source for districts and coastal practitioners that can provide both decadal and short-term shoreline insights at broad spatial scales. These satellite data can potentially reduce the costs associated with monitoring coastal management actions, improve project design and inform adaptive management and feasibility studies. The development of a user-friendly desktop tool to make this technology more accessible is ongoing.

6.2 Recommendations

The research team suggest a primary takeaway from this effort is that CoastSat shoreline accuracy is strongly linked to satellite pixel resolution. Despite the capability to operate at a subpixel scale, we hypothesize that consistent accuracy <5 m would be difficult to achieve without improved satellite resolution. Only one test site (South Padre 8) was <5 m accuracy.

Other work by Doherty et al. (2022) focused on PlanetScope imagery with a resolution of 3.0 m at Duck and other sites and found RMSEs ranging from 3.5 m to 5.1 m. Doherty et al. (2022; p. 11) states "the increase in accuracy obtained by PlanetScope imagery is subsequently sufficient to capture smaller-scale variability at the sub-annual or seasonal timescales, particularly considering the generally smaller magnitude of shoreline variability at Duck relative to Narrabeen. This was identified as a key limitation of applying CoastSat and Landsat/Sentinel-2 at less dynamic sites (Vos et al. 2019a)."

There are other higher resolution imagery candidates to consider as well including Maxar Worldview-3 (pixel resolution = 0.31 m) (Turner et al. 2021) and Dove Cubesats that are capable of multiple passes per day which could potentially help to reduce shoreline noise. These are currently not compatible within the CoastSat workflow.

Bibliography

Almeida, L. P., I. Efraim de Oliveira, R. Lyra, R. Scaranto Dazzi, V. Martins, and A. Henrique da Fontoura Klein. 2021. "Coastal Analyst System from Space Imagery Engine (CASSIE): Shoreline Management Module." *Environmental Modelling Software* 140. https://doi.org/10.1016/j.envsoft.2021.105033.

Aronow, S., W. Fisher, J. McGowen, and V. Barnes. 1982. "Geologic Atlas of Texas, Houston Sheet: The University of Texas at Austin, Bureau of Economic Geology, scale 1:250,000, 1 sheet." *The Bureau Store*. https://store.beg.utexas.edu/geologic-atlas-of-texas/2064-ga0018.html.

Bergsma, E., M. Sadio, I. Sakho, R. Almar, T. Garlan, M. Gosselin, and H. Gauduin. 2020. "Sand-Spit Evolution and Inlet Dynamics Derived from Space-Borne Optical Imagery: Is the Senegal-River Inlet Closing?" *Journal of Coastal Research*, SI-95: 372–376. http://dx.doi.org/10.2112/SI95-072.1.

Birkemeier W., R. Dolan, and N. Fisher. 1984. "The Evolution of a Barrier Island: 1930–1980." *Shore and Beach* 52 (3): 2–12.

Bishop-Taylor, R., R. Nanson, S. Sagar, and L. Lymburner. 2021. "Mapping Australia's Dynamic Coastline at Mean Sea Level Using Three Decades of Landsat Imagery." *Remote Sensing of Environment* 267. https://doi.org/10.1016/j.rse.2021.112734.

Brown, L., J. Brewton, J. McGowen, C. Proctor, S. Aronow, and V. Barnes. 1975. "Geologic Atlas of Texas, Beeville-Bay City Sheet: The University of Texas at Austin, Bureau of Economic Geology, scale 1:250,000, 1 sheet." *The Bureau Store*. https://store.beg.utexas.edu/geologic-atlas-of-texas/2092-ga0005.html.

Brown, S., J. W. Long, E. Himmelstoss, and A. S. Farris. 2021. "Using Satellite Data and the Kalman Filter to Improve Analysis of Historical Shoreline Trends from 1984 to the Present and Future Projections Along the US Atlantic Coast." M.S. thesis, University of North Carolina Wilmington. https://ui.adsabs.harvard.edu/abs/2020AGUFMOS038..05B/abstract.

Bruder, B., K. Brodie, N. Spore, A. Renaud, and K. Hodgens. 2019. "Continuous Monitoring of a Nearshore Berm Placement at New Smyrna Beach, FL Via Coastal Imagery." *Coastal Sediments*, 2443–2457. https://doi.org/10.1142/9789811204487_0209.

Castelle, B., G. Masselink, T. Scott, C. Stokes, A. Konstantinou, V. Marieu, and S. Bujan. 2021. "Satellite-Derived Shoreline Detection at a High-Energy Meso-Macrotidal Beach." *Geomorphology* 383. https://doi.org/10.1016/j.geomorph.2021.107707.

Chrzastowski, M., C. Foyle, and C.Trask. 1996. "Erosion and Accretion Trends Along the Lake Michigan Shore at North Point Marina and Illinois Beach State Park. Year-1 (1995) Report of a Four-Year Study of Coastal Geology and Coastal Geologic Processes." *Illinois State Geological Survey*: *Coastal and Wetlands Geology Section*. https://www.ideals.illinois.edu/items/44994.

Cialone, M., and E. Thompson. 2000. *Wave Climate and Littoral Sediment Transport Potential, Long Beach Island, New Jersey*. ERDC/CHL TR-00-21. Vicksburg, MS: US Army Corps of Engineers Engineer Research and Development Center–Coastal Hydraulics Laboratory. http://hdl.handle.net/11681/7451.

Cohn, N., K. Brodie, I. Conery, and N. Spore. 2022. "Alongshore Variable Accretional and Erosional Coastal Foredune Dynamics at Event to Interannual Timescales." *American Geophysical Union Earth and Space Science* 9(12). https://doi.org/10.1029/2022EA002447.

Dally, W., and D. Osiecki. 2018. "Evaluating the Impact of Beach Nourishment on Surfing: Surf City, Long Beach Island, New Jersey, U.S.A." *Journal of Coastal Restoration* 34 (4): 793–805. https://doi.org/10.2112/JCOASTRES-D-17-00162.1.

Doherty, Y., M. Harley, K. Vos, and K. Splinter. 2022. "A Python Toolkit to Monitor Sandy Shoreline Change Using High-Resolution PlanetScope Cubesats." *Environmental Modelling & Software* 157. https://doi.org/10.1016/j.envsoft.2022.105512.

Dolan R., H. Lins, B. Hayden. 1988. "Mid-Atlantic Coastal Storms." *Journal of Coastal Research* 4 (3): 417–433. https://www.jstor.org/stable/4297430.

Forte, M. F., W. Birkemeier, and R. Mitchell. 2017. *Nearshore Survey System Evaluation*. ERDC/CHL TR-17-19. Vicksburg, MS: Coastal Hydraulics Laortory–Engineer Research and Development Center. http://dx.doi.org/10.21079/11681/26031.

Fraser, G., C. Larsen, and N. Hester. 1990. "Climatic Controls of Lake Levels in the Lake Michigan and Lake Huron Basins." In *Late Quaternary history of the Lake Michigan basin: Geological Society of America Special Paper,* Schneider, A. F., and Fraser, G. S., eds., 251: 75–89. https://doi.org/10.1130/SPE251-p75.

Hagenaars, G., A Luijendijk, S. de Vries, and W. de Boer. 2017. Long term coastline monitoring derived from satellite imagery. *Coastal Dynamics* 122: 1551–1562. https://doi.org/10.1016/j.coastaleng.2017.12.011.

Holman, R., A. Sallenger, T. Lippmann, and J. Haines. 1993. "The Application of Video Image Processing to the Study of Nearshore Processes." *Oceanography* 6 (3): 78–85. https://www.jstor.org/stable/43924648.

Kaminsky, G., P. Ruggiero, M. Buijsman, D. Mccandless, and G. Gelfenbaum. 2010. "Historical Evolution of the Columbia River Littoral Cell". *Marine Geology* 273 (1–4): 96–126. https://doi.org/10.1016/j.margeo.2010.02.006.

LeBlanc, R., and W. Hodgson. 1959. "Origin and Development of the Texas shoreline." *Gulf Coast Association of Geological Societies Transactions* 9: 197–220. http://hdl.handle.net/1969.3/26078.

Lee, G., R. Nicholls, and W. Birkemeier. 1998. "Storm-Driven Variability of the Beach-Nearshore Profile at Duck, North Carolina, USA, 1981–1991." *Marine Geology* 148 (3–4): 163–177. https://doi.org/10.1016/S0025-3227(98)00010-3.

Lippmann, T. and R. Holman. 1989. "Quantification of Sand Bar Morphology: A Video Technique Based on Wave Dissipation." *Journal of Geophysical Research* 94 (C1): 995–1011. https://doi.org/10.1029/JC094iC01p00995.

Ludka, B., R. Guza, W. O'Reilly, M. Merrifield, R. Flick, A. Bak, T. Hesser, et al. 2019. "Sixteen Years of Bathymetry and Waves at San Diego Beaches." *Scientific Data* 6 (161). https://www.nature.com/articles/s41597-019-0167-6.

Luijendijk, A., G. Hagenaars, R. Ranasinghe, F. Bart, G. Donchyts, and S. Aarninkof. 2018. "The State of the World's Beaches." *Scientific Reports* 8 (6641): 1–11. https://www.nature.com/articles/s41598-018-24630-6.

McGill, S., B. Harris, B. McFall, D. Krafft, N. Bain, N. Olsen, N. I. Conery, and M. Chasten. 2022. "Morphological Analysis of a Nearshore Nourishment Along the Atlantic Coast of New Jersey, USA." *Journal of Marine Science and Engineering* 10 (11): 1622. https://doi.org/10.3390/jmse10111622.

Onnink, C., 2020. "Dynamic Shoreline Response to a Shallow Concentrated Nearshore Berm Nourishment." M.S. thesis, Delft University of Technology. https://repository.tudelft.nl/islandora/search/author%3A%22Onnink%2C%20C.J.%22.

Paine, J. G., and T. Caudle. 2020. *Shoreline Movement Along the Texas Gulf Coast, 1930s to 2019*. Contract No. 16-201-000, Work Order No. B428 CEPRA Project No. 1662. Austin, TX: Bureau of Economic Geology. https://www.beg.utexas.edu/files/content/beg/research/gulfShorelineUpdate2019_r03.pdf.

Paine, J., T. Caudle, and J. Andrews, J. 2021. *Shoreline Movement and Beach and Dune Volumetrics along the Texas Gulf Coast, 1930s to 2019*. Contract No. 16-201-000, Work Order B428, CEPRA Project No. 1662. Austin, TX: Bureau of Economic Geology. https://coastal.beg.utexas.edu/shorelinechange2019/assets/glo_gsu_2019_r02_d4.pdf.

Ruggiero, P., G. Kaminsky, G. Gelfenbaum and B. Voigt. 2005. "Seasonal to Interannual Morphodynamics along a High-Energy Dissipative Littoral Cell." *Journal of Coastal Research* 21 (3): 553–578. https://doi.org/10.2112/03-0029.1.

Scheffler D., A. Hollstein, H. Diedrich, K. Segl, and P. Hostert. 2017. "AROSICS: An Automated and Robust Open-Source Image Co-Registration Software for Multi-Sensor Satellite Data." *Remote Sensing* 9 (7):676. https://doi.org/10.3390/rs9070676.

Stapor, F., and J. May. 1983. "The Cellular Nature of Littoral Drift Along the Northeast Florida Coast." *Marine Geology* 51 (3-4): 217–237. https://doi.org/10.1016/0025-3227(83)90105-6.

Stockdon, H., A. Sallenger, R. Holman, and P. Howd. 2007. "A Simple Model for the Spatially-Variable Coastal Response to Hurricanes." *Marine Geology* 238 (1-4): 1–20. https://doi.org/10.1016/J.MARGEO.2006.11.004.

Storey, J., D. Roy, J. Masek, F. Gascon, and M. Choate. 2016. "A Note on the Temporary Misregistration of Landsat-8 Operational Land Imager (OLI) and Sentinel-2 Multi Spectral Instrument (MSI) Imagery." *GSCE Faculty Publications* 186: 121–122. https://openprairie.sdstate.edu/gsce_pubs/35.

Storey, M. Choate, K. Lee Landsat-8 Operational Land Imager on-orbit geometric calibration and performance Remote Sens., 6 (11) (2014), pp. 11127-11152, 10.3390/rs61111127 https://sentinel.esa.int/documents/247904/4598066/Sentinel-3-OLCI-Land-Handbook.pdf.

Theuerkauf, E., K. Braun, D. Nelson, M. Kaplan, S. Vivirito, and J. Williams. 2019. "Coastal Geomorphic Response to Seasonal Water-Level Rise in the Laurentian Great Lakes: An Example from Illinois Beach State Park, USA." *Journal of Great Lakes Research* 45 (6), 1055–1068. https://doi.org/10.1016/j.jglr.2019.09.012.

Thompson, E. 1977. "Wave climate at selected locations along US coasts." TR 77-1. Ft. Belvoir, Virginia: US Army Corps of Engineers–Coastal Engineering Research Center. https://apps.dtic.mil/sti/pdfs/ADA037904.pdf.

Tondewad, P., and D. Manisha. 2020. "Remote Sensing Image Registration Methodology: Review and Discussion." *Procedia Computer Science* 171: 2390–2399. https://doi.org/10.1016/j.procs.2020.04.259.

Trémas, T., C. Déchoz, S. Lacherade, J. Nosavan, and B. Petrucci. 2015. "Sentinel-2: Presentation of the CAL/VAL Commissioning Phase." *Proceedings: SPIE Remote Sensing* 9643. https://doi.org/10.1117/12.2194847.

Velasquez-Montoya, L., M. Overton, and E. Sciaudone. 2020. "Natural and Anthropogenic-Induced Changes in a Tidal Inlet: Morphological Evolution of Oregon Inlet." *Geomorphology* 350. https://doi.org/10.1016/j.geomorph.2019.106871.

Vos, K., M. Harley, K. Splinter, A. Walker, and I. Turner. 2020. "Beach Slopes from Satellite-Derived Shorelines." *Geophysical Research Letters* 47 (14). https://doi.org/10.1029/2020GL088365.

Vos, K., M. Harley, K. Splinter, J. Simmons, and I. Turner. 2019. "Sub-Annual to Multi-Decadal Shoreline Variability from publicly Available Satellite Imagery." *Coastal Engineering* 150: 160-174. https://doi.org/10.1016/j.coastaleng.2019.04.004.

Wright, L and A. Short. 1984. "Morphodynamic Variability of Surf Zones and Beaches: A Synthesis. *Marine Geology* 56 (1–4): 93–118. https://www.researchgate.net/publication/238375548_Morphodynamic_variability_of_surf_zones_and_beaches_A_synthesis.

Xu, N., 2018. "Detecting Coastline Change with All Available Landsat Data over 1986–2015: A Case 835 Study for the State of Texas, USA." *Atmosphere* 9 (3): 107. https://doi.org/10.3390/atmos9030107.

Abbreviations

AROSICS	Automated and Robust Open-Source Image Co-Registration Software for Multi-Sensor Satellite Data
CHL	Coastal and Hydraulics Laboratory
CODS	Coastal Ocean Data Systems
CRLC	Columbia River Littoral Cell
CSRM	Coastal storm risk management
DEM	Digital elevation model
ERDC	Engineer Research and Development Center
FRF	Field Research Facility
GEE	Google Earth Engine
GIS	Geographical information systems
GNSS	Global Navigation Satellite System
Hs	Significant wave height
LE90	Linear error with 90% confidence
ML	Machine learning
MNDWI	Modified normalized difference water index
n/a	Not available
NAP	Philadelphia District
NAVD 88	North American Vertical Datum of 1988
NDBC	National Data Buoy Center
NDWI	Normalized difference water index
QAQC	Quality assurance and quality control

RMSE	Root-mean-square error
RTK	Real-time kinematic
SAJ	Jacksonville District
SPAW	Shoreward propagating accretionary wave
SWIR	Short-wave infrared
UAV	Unmanned aerial vehicle
USACE	United States Army Corps of Engineers
WRDA	Water Resources Development Act

REPORT DOCUMENTATION PAGE

1. REPORT DATE	2. REPORT TYPE	3. DATES COVERED	
June 2024	Final Report	START DATE FY22	END DATE FY23

4. TITLE AND SUBTITLE

Quantifying Coastal Evolution and Project Performance at Beaches by Using Satellite Imagery

5a. CONTRACT NUMBER	5b. GRANT NUMBER	5c. PROGRAM ELEMENT
5d. PROJECT NUMBER	**5e. TASK NUMBER**	**5f. WORK UNIT NUMBER**

6. AUTHOR(S)

Ian W. Conery, Nicholas R. Olsen, Shannon Brown, and Katherine L. Brodie

7. PERFORMING ORGANIZATION NAME(S) AND ADDRESS(ES)

US Army Engineer Research and Development Center
Coastal Hydraulics Laboratory
3909 Halls Ferry Road
Vicksburg, MS 39180-6199

8. PERFORMING ORGANIZATION REPORT NUMBER

ERDC/CHL TR-24-14

9. SPONSORING/MONITORING AGENCY NAME(S) AND ADDRESS(ES)

Coastal and Hydraulics Laboratory
3909 Halls Ferry Road
Vicksburg, MS 39180-6199

10. SPONSOR/MONITOR'S ACRONYM(S)

11. SPONSOR/MONITOR'S REPORT NUMBER(S)

12. DISTRIBUTION/AVAILABILITY STATEMENT

Distribution Statement A. Approved for public release: distribution is unlimited.

13. SUPPLEMENTARY NOTES

AMSCO 060000, "CODS/CIRP CoastSat"

14. ABSTRACT

Accurately delineating the shoreline is crucial for tracking coastal evolution, community vulnerability, storm impacts, and for coastal management decision-making. However, existing shoreline measurement methods are often time-consuming and expensive and therefore, USACE Districts are often forced to narrow areas of interest or monitoring frequency, decreasing the likelihood of making data-driven management decisions, especially over regional scales. In the last decade, space-borne earth observations have captured images subweekly, and can potentially be used for shoreline monitoring. This work investigated the Python-based CoastSat toolkit and compared the shorelines derived from publicly available satellite imagery to ground truth surveys at 37 sites across the nation chosen in coordination with Districts. Mean horizontal errors ranged from 4.21 to 20.58 m with an overall mean of 11.32 m. Tidal corrections improved accuracies at 82% of sites. The CoastSat slope function was tested and there were negligible differences in shoreline accuracy when compared with user-defined slopes Twenty-year satellite-derived trends generally align well with ground truth trends. The satellite approach identified quantifying storm impacts/recovery, beach nourishment equilibration, diffusion and decay, shoreline response to nearshore berm placements and decadal shoreline evolution at the evaluated district sites. Work is ongoing to transition to a user-friendly software tool.

15. SUBJECT TERMS

Coastal management; Coastal monitoring; GIS (Geographic information systems); Remote sensing; Satellite-derived shorelines; Shoreline mapping; Storm impact assessment

16. SECURITY CLASSIFICATION OF:			17. LIMITATION OF ABSTRACT	18. NUMBER OF PAGES
a. REPORT	b. ABSTRACT	C. THIS PAGE		
Unclassified	Unclassified	Unclassified	SAR	79

19a. NAME OF RESPONSIBLE PERSON	19b. TELEPHONE NUMBER (include area code)
Ian W. Conery	(252) 261-6840